Eddy-Mean Flow Interactions Sustaining the Anomalous Deep Convection off Prydz Bay in the Subpolar Southern Ocean

Yunzhu He[1,2], Dujuan Kang[1*], Karen J. Heywood[2*], and Meng Zhou[1,3]

[1] State Key Laboratory of Submarine Geoscience; Key Laboratory of Polar Ecosystem and Climate Change, Ministry of Education; Shanghai Key Laboratory of Polar Life and Environment Sciences; and School of Oceanography, Shanghai Jiao Tong University, 1954 Huashan Road, Shanghai, China

[2] Centre for Ocean and Atmospheric Sciences, School of Environmental Sciences, University of East Anglia, Norwich, UK

[3] Key Laboratory for Polar Science, Polar Research Institute of China, Ministry of Natural Resources, Shanghai, China

Correspondence to: D. Kang and K. Heywood, kangdj@sjtu.edu.cn; K.Heywood@uea.ac.uk

Key Points

- An eddy event associated with deep convection is identified off Prydz Bay, linking surface forcing to subsurface ocean variability.
- The vertical dynamics are sustained by combined surface divergence and eddy-driven vertical energy fluxes from depths > 1000 m.
- The resulting deep-ocean responses exhibit a zonally asymmetric circulation in the subpolar region, modulated by eddies.

Abstract

A remarkable deep-convection event developed off Prydz Bay in the Indian sector of the Southern Ocean during the austral autumn-winter of 2017, coinciding with a previously documented anomalous accumulation of eddy kinetic energy. During this event, warm Circumpolar Deep Water (CDW) shoaled toward the upper ocean despite strong surface stratification typically associated with sea-ice meltwater that suppresses vertical mixing. Using an eddy-resolving reanalysis data set and an energetics-based diagnostic framework, we investigate the processes linking atmospheric forcing, eddy variability, and deep convection. The results suggest a dynamic system in which anomalous surface forcing initiates upper-ocean divergence and preconditioning, followed by intensified mesoscale eddy activity and vertical energy redistribution. These processes together contribute to the development of deep convection and CDW uplift. Enhanced CDW intrusion is accompanied by intensified baroclinic conversion near the continental slope, consistent with eddy growth and enhanced vertical energy convergence. The associated eddy-mean flow interactions correspond to isopycnal steepening and pronounced southward transport anomalies, producing a zonally asymmetric circulation pattern in the subpolar region. These results highlight that, in addition to atmospheric forcing, energetic eddies play a key role in sustaining vertical exchange and enabling convection to extend to depths approaching 2000 m. Such intense events can substantially modify regional circulation and water-mass properties and influence heat and salt redistribution in polar oceans. Understanding these dynamics is essential for improving climate models and predicting future changes in subpolar ocean circulation.

Plain Language Summary

In 2017, an anomalously strong eddy event occurred near Prydz Bay in East Antarctica, a region where warm Circumpolar Deep Water (CDW) interacts with colder shelf waters and influences regional ocean circulation. During this event, intense ocean eddies coincided with signals of deep convection, indicating enhanced vertical exchange between the deep ocean and upper layers. Normally, melting sea ice makes the ocean surface fresher and stabilizes the water column, which limits vertical mixing. During this event, however, changes in wind patterns together with intensified ocean eddies helped maintain the uplift of CDW. Using high-resolution reanalysis data, we show that atmospheric disturbances triggered changes at the surface layer that were linked to deeper ocean processes through mesoscale eddies. These eddies redistributed heat and energy within the water column and contributed to convection reaching depths of nearly 2000 m. These findings highlight the important role of eddies in

connecting upper ocean variability with deep dynamics in the subpolar Southern Ocean. These eddies are poorly represented in coarse-resolution climate models but are essential for understanding and predicting future changes in ocean circulation and climate.

1. Introduction

The Antarctic continental margin is a region of intense oceanic activity where large-scale circulation, mesoscale processes, and climate variability interact to regulate cross-shelf exchange and water-mass distribution [Whitworth III et al., 1985; Thompson et al., 2018]. In the Southern Ocean, Circumpolar Deep Water (CDW) is transported southward toward the Antarctic continental slope, where it shoals along the shelf break and influences heat and salt distributions near the continental margin, sustaining coastal polynya activity and ice-shelf basal melt [Nunes Vaz and Lennon, 1996; Thompson et al., 2014; Morrison et al., 2020]. Strengthened and poleward-shifted westerlies in recent decades have enhanced CDW upwelling near the continental slope, contributing to increased subsurface warming [Spence et al., 2014; Schmidtko et al., 2014]. These changes are essential for both ice-sheet mass balance and the regulation of nutrient supply and biological productivity. However, these cross-shelf exchange processes vary significantly among Antarctic sectors [Thompson et al., 2018], highlighting the need for localized investigations to resolve the specific dynamics governing regional circulation.

The Prydz Bay region (Figure 1), including the Cooperation Sea (60°–80°E), in the Indian sector of the Southern Ocean, is recognized as one of the major hotspots of Antarctic Bottom Water (AABW) formation [Ohshima et al., 2013; Williams et al., 2016; Silvano et al., 2023]. Regional gyre circulation and slope processes shape a dynamically connected system in which dense shelf water (DSW) formed in the Cape Darnley polynya and the inflow of CDW interact to regulate cross-shelf exchange. To the west, the Cape Darnley polynya (65°–69°E) produces cold, saline DSW through intense winter cooling and brine rejection, which cascades off the continental slope to ventilate the abyssal ocean and contribute to AABW formation [Williams et al., 2016; Blanckensee et al., 2024]. In contrast, in the eastern sector near Prydz Bay, CDW shoals to the continental slope and mixes with shelf waters to form modified Circumpolar Deep Water (mCDW). Once onto the shelf, mCDW interacts with cold shelf waters, influencing sea-ice production, sub-ice shelf melting, and dense water formation [Smith et al., 1984; Liu et al., 2017; Guo et al., 2022].

Cross-shelf exchange and vertical heat redistribution in this region are strongly mediated by mesoscale eddies and turbulent mixing, which act along energetic fronts and steep density gradients near the shelf break [Nøst et al., 2011; Thompson et al., 2014; Stewart and Thompson, 2015]. Recent observations have shown marked interannual variability in CDW intrusion pathways and water-mass properties near Prydz Bay, with wind forcing and eddy activity identified as key modulators [Rintoul, 2018; Zu et al., 2022]. Intensified summer winds can enhance mCDW shoaling along bathymetric features, while buoyancy-driven upwelling and winter convection associated with surface cooling and sea ice formation further lift intruded waters and weaken the stratification of shelf waters through vertical mixing [Guo et al., 2019; Guo et al., 2022]. These processes highlight the importance of mesoscale variability and vertical mixing in modulating cross-shelf exchange and the redistribution of intruding CDW in this region. However, previous studies have emphasized wind-driven variability and the pathways of CDW intrusions within the continental shelf region. In contrast, the outer continental slope region, where mesoscale eddy activity is more energetic, remains less explored. In particular, the role of eddy energetics and their interaction with deep convection processes remains poorly understood. This study addresses this gap by examining an anomalous event and investigating how eddies interact with convection processes to redistribute heat vertically and modulate CDW uplift near Prydz Bay.

Building on the regional background, a strong eddy event occurred near Prydz Bay in 2017 (Figure 1), providing a unique case for investigating the coupled processes. This event followed the pronounced 2016–2017 Antarctic sea-ice decline, during which sea-ice extent decreased rapidly from September 2016 and reached a record low in December, coinciding with anomalously warm surface waters surrounding much of Antarctica [Stuecker et al., 2017; Meehl et al., 2019; Wang et al., 2019]. This abrupt sea-ice retreat has been interpreted as a potential shift in Southern Ocean climate variability [Purich et al., 2023]. Enhanced mesoscale eddy activity has also been associated with regional ocean warming, suggesting that similar processes may become more relevant under future climate change [He et al., 2023]. In the Indian sector of the Southern Ocean, regional warming and associated hydrographic anomalies were also reported near Prydz Bay [Meehl et al., 2019; Sabu et al., 2021]. During the subsequent autumn and winter of 2017 (seasons here follow the Southern Hemisphere convention: austral summer refers to January–March), regionally intense enhancement of eddy kinetic energy (EKE) developed near the Prydz Bay continental slope. The oceanic anomaly, therefore, provides an opportunity to examine how mesoscale processes respond to large-scale climatic perturbations.

Using an energetics framework, He et al. [2024] showed that this anomalous eddy activity was primarily generated through baroclinic conversion from mean potential energy to eddy energy, associated with anomalous CDW intrusions and enhanced Ekman pumping. The results indicated that internal baroclinic processes dominated in energizing mesoscale variability during this event. However, identifying the source of the anomalous eddy energy does not explain its broader impact on the water column. It remains unclear how this large reservoir of eddy energy interacts with stratification and how heat and energy are redistributed vertically. Addressing these questions is essential for understanding how mesoscale variability influences vertical exchange and water-mass structure near the continental margin. In this study, we extend the energetics framework of He et al. [2024] by incorporating diagnostics of vertical pressure-flux divergence to examine vertical energy redistribution and applying a convective proxy to quantify the depth of mixing. The results reveal a dynamically linked sequence of processes in which anomalous surface forcing initiates upper-ocean divergence and preconditioning, while enhanced mesoscale eddies and associated vertical energy fluxes sustain vertical exchange and enable deep convection in this climatically sensitive region.

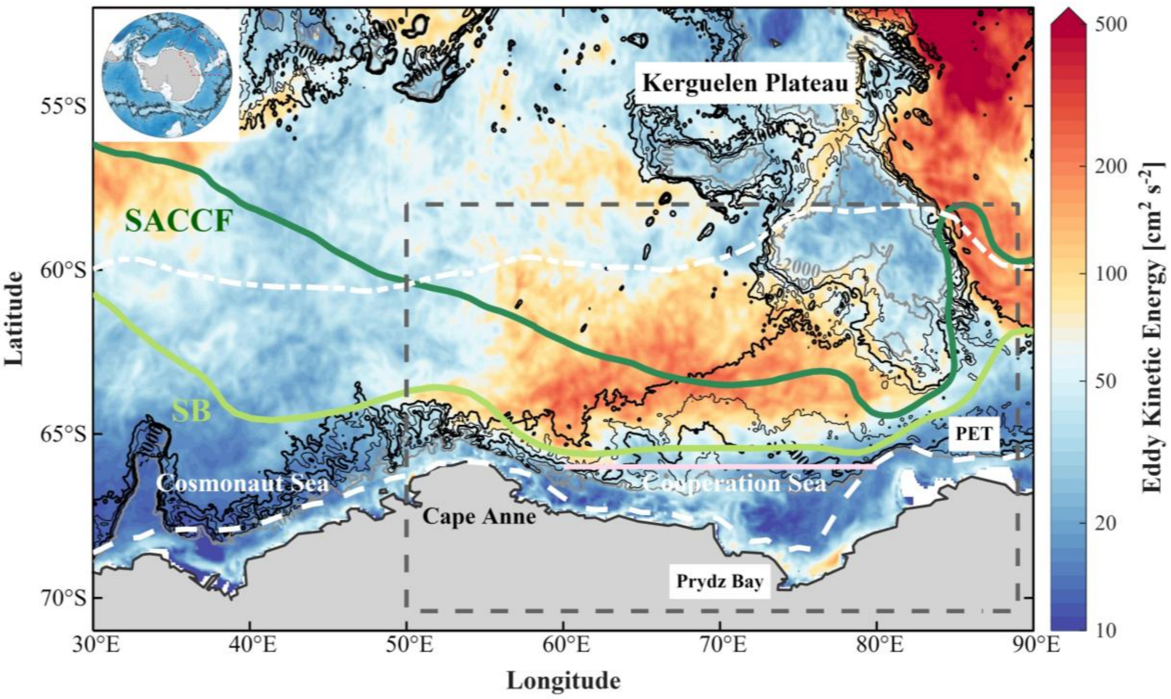

Figure 1. Spatial distribution of eddy kinetic energy (EKE) in 2017 in the Kerguelen-Indian sector of the Southern Ocean, overlaid with bathymetric contours and schematic positions of major oceanic fronts and currents. Colors are shown on a logarithmic (log10) scale to highlight the visibility of high-energy regions. The Cooperation Sea and Prydz Bay form the key focus region of this study (dashed gray box), covering the Antarctic continental margin where mesoscale eddies, slope currents, and subpolar gyre circulation interact. EKE derived from the GLORYS12V1 reanalysis data highlights elevated mesoscale activity downstream

of the Kerguelen Plateau and along the Southern ACC Front (SACCF), with emphasis here on the margin region. The 66°S transect (60°E–80°E) used for the transport calculation in Figure 4 is marked by a pink line, located near the 1000 m isobath along the continental slope. Bathymetry is shown in black contours at 500 m intervals, with the 2000 m isobath emphasized in light gray based on the ETOPO 2022 15 Arc-Second Global Relief Model (NOAA National Centers for Environmental Information, 2022). Major hydrographic fronts are indicated by green solid lines, including the SACCF, and the Southern Boundary of the ACC (SB), following Park et al. [2019]. The winter and summer sea ice extent are denoted by the white dot-dashed line and white dashed line, following Comiso et al. [2003]. The Princess Elizabeth Trough (PET; 63°–66° S, ~85° E) acts as a major bathymetric gateway for cross-shelf exchange.

2. Data and Methods

2.1. Data

The oceanic dataset used in this study is the Global Ocean Reanalysis and Simulation 12v1 (GLORYS12V1) product from the Copernicus Marine Environment Monitoring Service (CMEMS), with a horizontal resolution of 1/12° (~4.2 km in the adjacent Cooperation Sea region) and 50 vertical levels covering the altimetry era (1993–2021). This resolution is comparable to the first baroclinic Rossby radius (~ 5 km) in many parts of the Southern Ocean (Huntley & Niiler, 1995), allowing mesoscale variability to be represented at regional scales. As the present analysis focuses on regional eddy variability and energetics rather than individual eddy structures, the resolution is considered sufficient for the analysis. The GLORYS12V1 has been applied in studies of Southern Ocean energetics and Antarctic coastal water-mass transformation, and its performance has been validated in reproducing the energy structure near the Prydz Bay region [Oelerich et al., 2022; He et al., 2024]. The reanalysis is based on the Nucleus for European Modelling of the Ocean (NEMO, version 3.6) model, initially forced by the European Center for Medium-Range Weather Forecasting interim reanalysis (ERA-Interim, 1993–2018) atmospheric fields and later transitioned to ERA5 (2019–2021).

To represent surface forcing, we employed 10-m wind fields from the ERA5 reanalysis, covering the period from 1993 to 2021 with a spatial resolution of 0.25°. These wind data were used to calculate wind stress and wind stress curl, and, in combination with GLORYS12V1 sea-ice concentration fields, to derive Ekman divergence (i.e., Ekman pumping/suction). For the wind-related analysis, ocean variables were bilinearly interpolated onto the ERA5 grid to ensure spatial consistency with the atmospheric fields. Sea ice modulates air-sea momentum transfer by altering the effective surface stress [Timmermann et al., 2009]. To account for this effect, total surface stress over regions partially covered by sea ice is represented as a combination of wind stress over open water ($\vec{\tau}_{\mathrm{ao}}$) and ice-ocean stress ($\vec{\tau}_{\mathrm{io}}$). This approach distinguishes the open-water wind stress from the total atmospheric surface stress [Wu et al., 2021; Wang et al., 2023].

The wind stress over open water is estimated using the quadratic drag law, derived from

$$\vec{\tau}_{\mathrm{ao}} = \rho_{\mathrm{a}} C_{\mathrm{D,ao}} \left|\vec{U}_{10}\right| \vec{U}_{10}, \tag{1}$$

where ρ_{a}= 1.29 kg m^{-3} is the air density, and $\vec{U}_{10} = (u_{10}, v_{10})$ is the 10-m wind vector. The air-ocean drag coefficient $C_{\mathrm{D,ao}}$ follows a piecewise formulation [Wang et al., 2023]:

$$C_{\mathrm{D,ao}} = \begin{cases} 1.2 \times 10^{-3}, \left|\vec{U}_{10}\right| < 11\ \mathrm{m\ s^{-1}} \\ \left(0.49 + 0.065\left|\vec{U}_{10}\right|\right) \times 10^{-3}, 11\mathrm{m\ s^{-1}} \leq \left|\vec{U}_{10}\right| \leq 25\ \mathrm{m\ s^{-1}} \end{cases}. \tag{2}$$

The ice-ocean surface stress is calculated as:

$$\vec{\tau}_{\mathrm{io}} = \rho_w C_{\mathrm{D,io}} \left|\vec{U}_{\mathrm{ice}} - \vec{U}_{\mathrm{w}}\right| \left(\vec{U}_{\mathrm{ice}} - \vec{U}_{\mathrm{w}}\right), \tag{3}$$

where the seawater density is taken as $\rho_{\mathrm{w}} = 1026\mathrm{kg \cdot m^{-3}}$. The vectors $U_{\mathrm{ice}} = (u_{\mathrm{ice}}, v_{\mathrm{ice}})$ and $\vec{U}_{\mathrm{w}} = (u_{\mathrm{w}}, v_{\mathrm{w}})$ represent the velocities of sea ice and surface ocean currents, respectively. The influence of the turning angle between stress and velocity was considered negligible. The ice-ocean drag coefficient is set as $\mathrm{C_{D,io}} = 3.0 \times 10^{-3}$, which accounts for ice concentration, thickness, floe size, surface and basal roughness, and the presence of ridges.

The overall ocean surface stress over regions partially covered by sea ice is then computed as the area-weighted sum of wind-driven stress and ice-driven stress based on the sea ice concentration A (0–1) [Timmermann et al., 2009]. It is computed as follows:

$$\vec{\tau}_{\mathrm{o}} = A \cdot \vec{\tau}_{\mathrm{io}} + (1 - A) \cdot \vec{\tau}_{\mathrm{ao}}, \tag{4}$$

Based on the total stress field, the Ekman vertical velocity (i.e., Ekman pumping/suction) is calculated as the divergence of the Ekman transport:

$$W_{ek} = \partial/\partial \mathrm{x}\left(\vec{\tau}_{\mathrm{o}}{}^{(\mathrm{y})}/(\rho f)\right) - \partial/\partial \mathrm{y}\left(\vec{\tau}_{\mathrm{o}}{}^{(\mathrm{x})}/(\rho f)\right) = \boldsymbol{k} \cdot \nabla \times (\vec{\tau}_{\mathrm{o}}/\rho f), \quad (5)$$

where $\boldsymbol{k}$ is the vertical unit vector, and f is the Coriolis parameter. In the Southern Hemisphere (where $f < 0$), negative wind stress curl induces Ekman upwelling (suction), while positive curl induces downwelling. Anomalies in this study are referenced to the 2010–2020 monthly climatology, excluding 2017 to avoid contaminating the baseline with the extreme year on which the study focuses.

Hydrological variables, including potential temperature θ, practical salinity S, and neutral density (γ_{n}) are used to identify water masses. Following Meijers et al. [2010], CDW is defined within a neutral density (γ_{n}) range of $28.03 < \gamma_{\mathrm{n}} < 28.27$ (kg m^{-3}).

2.2. Energetics Framework

To investigate the dynamics underlying the anomalous upwelling of CDW and associated deep convection, we adopt the energetics framework as used by He et al. [2024] and extend it by incorporating vertical pressure flux divergence to quantify the dynamic process of energy transfer in the subsurface and deeper layers [Kang and Curchitser, 2015; Jüling et al., 2018; Matsuta and Masumoto, 2023].

We consider a variable x decomposed into its temporal mean and eddy perturbation as $x = \bar{x} + x'$, where $\bar{x}$ denotes the temporal (e.g., monthly) mean and x' is the deviation from that mean. This Reynolds decomposition underpins the energetics framework applied in this study. The full energy budget consists of both kinetic energy and available potential energy (APE) components, which can be further separated into mean and eddy parts: mean kinetic energy (MKE), EKE, mean potential energy (MPE), and eddy potential energy (EPE). Although establishing a complete energy budget that includes all reservoirs and their interactions is complex, our analysis focuses on the key conversion terms that are dynamically most relevant to the anomalous convection process. Total seawater density $\rho(x, y, z, t)$ is defined as:

$$\rho(x, y, z, t) = \rho_r(z) + \rho_a(x, y, z, t), \quad (6)$$

where $\rho_r(z)$ is the reference density, the spatial and temporal mean of selected subregion at each depth, and ρ_a is the perturbation component. A constant reference density $\rho_0 = 1026$ kg m^{-3} is used for normalization. The squared buoyancy frequency is calculated by:

$$N^2 \equiv -\frac{g}{\rho_0}\frac{d\rho_r}{dz}, \quad (7)$$

where g is gravitational acceleration. A sensitivity test confirmed that using a regional constant N at each depth is sufficient to capture stratification patterns in the study area. With these definitions, energy components are estimated as follows:

$$\mathrm{MKE} = \frac{1}{2}(\bar{u}^2 + \bar{v}^2), \tag{8}$$

$$\mathrm{EKE} = \frac{1}{2}(u'^2 + v'^2), \tag{9}$$

$$\mathrm{MPE} = \frac{g^2 \bar{\rho}_a^2}{2{\rho_0}^2 N^2}, \tag{10}$$

$$\mathrm{EPE} = \frac{g^2 \rho_a'^2}{2{\rho_0}^2 N^2}, \tag{11}$$

where the overbar (−) denotes a time average over one month in this study, and prime (′) denotes departures of daily variables from their respective monthly means. We adopt a 1-month averaging window, ensuring that MKE reflects the monthly mean flow energy, while EKE captures contributions from transient eddies and submonthly disturbances. To standardize units, all energy expressions are normalized by ρ_0, yielding values in m^2 s^{-2} (reported in cm^2 s^{-2}). Following the orthogonal decomposition approach of Kang and Curchitser [2017], this framework reliably separates the physically consistent mean and eddy energy components [He et al., 2024].

The conversion from potential to kinetic energy is a fundamental process sustaining mesoscale and submesoscale variability in the Southern Ocean. In the baroclinic pathway, available MPE is released through isopycnal tilting and eddy buoyancy fluxes, transferring energy from MPE to EPE via the baroclinic conversion term (BCR), and subsequently from EPE to EKE through the vertical eddy density flux (VEDF). The barotropic pathway reflects the direct extraction of kinetic energy from the mean flow through horizontal shear instabilities, quantified by the barotropic conversion term (BTR). These energy conversions are diagnosed as

$$\text{Baroclinic:} \begin{cases} \mathrm{MPE} \to \mathrm{EPE}: \mathrm{BCR} = -\frac{g^2}{\rho_0^2 N^2} \overline{\rho_a' \boldsymbol{u}'} \cdot \nabla \overline{\rho_a}, \\ \mathrm{EPE} \to \mathrm{EKE}: \mathrm{VEDF} = -\frac{g}{\rho_0} \overline{{\rho_a}' w'}, \end{cases} \tag{13}$$

$$\text{Barotropic:} \quad \mathrm{MKE} \to \mathrm{EKE}: \ \mathrm{BTR} = -[\overline{u' \boldsymbol{u}'} \cdot \nabla \bar{u} + \overline{v' \boldsymbol{u}'} \cdot \nabla \bar{v}], \tag{14}$$

where $\boldsymbol{u}' = (u', v')$ is the horizontal eddy velocity components, and w' is the time-varying component of vertical velocity derived from the continuity equation following the Boussinesq approximation.

2.3. Vertical Pressure Flux and Divergence

To examine the vertical exchange of energy associated with deep convection and eddy-induced processes, and to establish a dynamical link between subsurface eddy activity and surface-layer anomalies observed during the 2017 event, we further diagnose the three-dimensional eddy pressure flux within the established energy framework, following Matsuta and Masumoto [2023]. The divergence of this flux,

$$\nabla \boldsymbol{\Phi}_p = \nabla_h \cdot (\overline{\boldsymbol{u}'p'}) + \partial_z(\overline{w'p'}), \tag{15}$$

quantifies the divergence by the eddy pressure flux, where p' is the pressure perturbation. The first term on the right represents the divergence of horizontal eddy pressure flux, while the second term indicates the vertical energy exchange between ocean layers [Zhai and Marshall, 2013; Matsuta and Masumoto, 2023]. This term reflects the vertical divergence of eddy pressure work, indicating whether energy is locally redistributed within the water column. Positive values of $\partial_z(\overline{w'p'})$ correspond to energy divergence (loss from the layer), whereas negative values indicate energy convergence (gain within the layer), associated with eddy-driven vertical buoyancy fluxes or energy release from deeper layers. The divergence of eddy advection, $-\nabla \cdot [\bar{\boldsymbol{u}}\mathrm{EKE} + \overline{\boldsymbol{u}'\mathrm{EKE}}]$, is also examined as an additional diagnostic check of EKE redistribution.

2.4. Volume and Heat Transport

In the present study, we focus on the poleward transport of water masses and associated heat content across the Antarctic continental slope. Poleward volume and heat transports across selected sections are evaluated by integrating meridional velocity and potential temperature over the selected vertical range. These diagnostics allow us to quantify both monthly variability and interannual anomalies associated with deep processes.

The meridional volume transport Q_V is defined as:

$$Q_V = \iint \ v \,\mathrm{d}z\, \mathrm{d}x, \tag{16}$$

where v is the meridional velocity, and the integration is taken over depth z and zonal distance x. The results are expressed in Sverdrups (1 Sv = 10^6 $\mathrm{m^3 s^{-1}}$).

The meridional heat transport Q_H is estimated following the classical heat budget formulation:

$$Q_H = C_P \rho_0 \iint \ v \cdot (\theta - \theta_{\mathrm{ref}}) \mathrm{d}z \ \mathrm{d}l, \tag{17}$$

where C_P is the heat capacity of seawater taken as 3990 J $\mathrm{kg^{-1}}$ $\mathrm{K^{-1}}$ in this study, v is the meridional velocity component, θ is the potential temperature, and dl is the unit distance along selected lateral boundaries. The reference potential temperature θ_{ref} is taken as 0 °C. Eddy heat fluxes from daily anomalies are reference independent. This formulation captures the net enthalpy flux relative to a background state, allowing attribution of heat convergence to variability in velocity, temperature, or both. Monthly values of Q_H and Q_V are computed to analyze temporal variability. Zonal-mean vertical profiles of heat flux are then derived to reveal the vertical structure of meridional heat transport.

2.5. Subsurface Convection Metric

To assess the vertical extent of convective mixing beneath the surface layer, Subsurface Convection Depth (SCD) is defined as the depth below 500 m at which the vertical gradient of neutral density reaches a local maximum. It indicates the deepest point of significant vertical homogenization associated with convection:

$$\mathrm{SCD} = \max_{z > 500\mathrm{m}} \left(\left| \frac{\partial \gamma_n}{\partial z} \right| \right). \tag{18}$$

This metric provides an estimate of the lower boundary of active vertical convection by detecting the depth of the strongest vertical density transition beneath the upper stratified layer. It is particularly useful in subpolar gyre systems such as Prydz Bay, where subsurface convection is influenced by both buoyancy forcing and interactions between warm CDW and cold shelf waters. Although temperature-based criteria are commonly used to identify convection, we found that vertical temperature gradients are primarily concentrated in the upper 200 m, where seasonal stratification and surface heating dominate. Since our focus is on deeper convective processes and their role in subsurface water mass transformation, the use of density offers a more reliable indicator of dynamic stability at depth, independent of salinity-compensated temperature variations. The 500 m threshold was thus selected to exclude surface-layer variability and isolate convective signals associated with deep overturning, particularly during austral winter when CDW-DSW interactions intensify. Seasonal and spatial variations in SCD are used in this study to track the penetration of deep convection and its modulation by mesoscale eddies and bathymetric features.

3. Results

3.1. Anomalous Uplift of Subsurface Warm Water

In 2017, concurrent with enhanced EKE (Figure 1), pronounced uplift of density surfaces occurred along the continental slope region between 60° and 80° E, accompanied by a subsurface warm anomaly originating from the north (Figure 2). The three-dimensional view illustrates the vertical hydrographic structure (Figure 2a). Along the meridional section at 72.5°E and zonal sections at 65°S (Figures 2b–i), isopycnals within the upper 500 m bulge upward compared with the climatology, with co-located warm anomalies in potential temperature. Systematic shoaling is pronounced during the austral autumn. The γ^n = 28.03 kg m^{-3} surface, commonly used to mark the upper boundary of CDW [Meijers et al., 2010; Guo et al., 2022], is several hundred meters shallower than its climatology (excluding 2017). The full seasonal variation of potential temperature along 72.5°E is shown in Figure S1. Here, we focus on April–July, when the anomaly develops. These hydrographic changes indicate a substantial restructuring of the subsurface stratification during 2017.

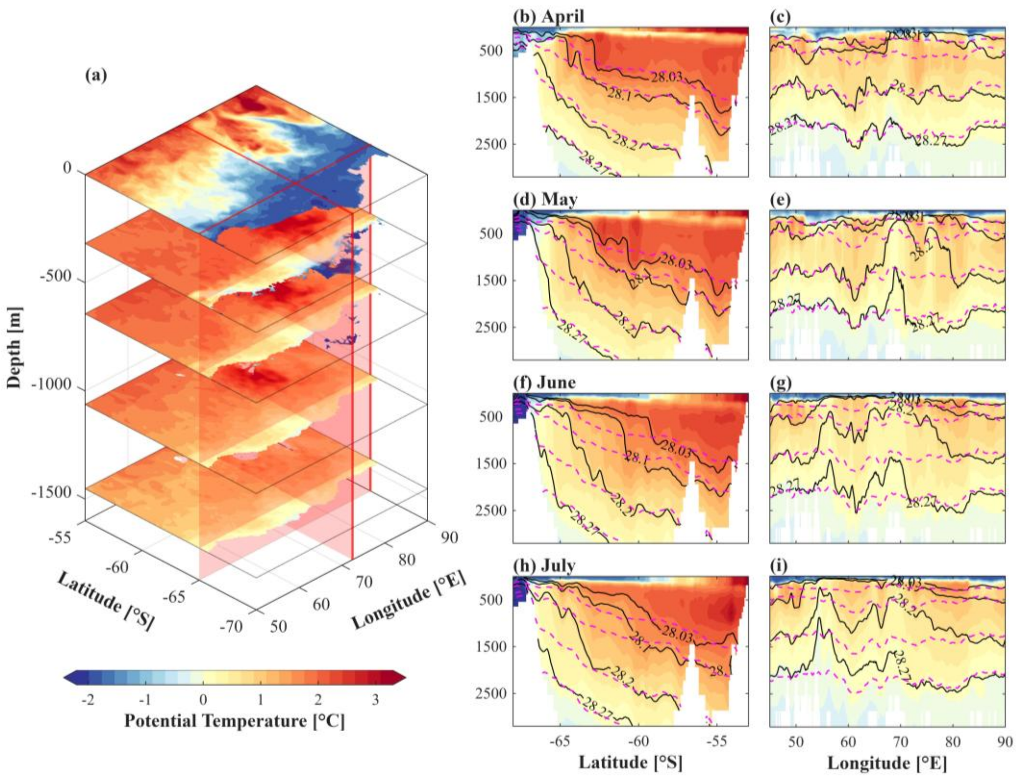

Figure 2. Hydrographic structure associated with the 2017 anomaly in the region indicated by the gray box in Figure 1. (a) Three-dimensional distribution of potential temperature in June 2017 across five depth layers from the surface to 1600 m. The light-red vertical planes mark the locations of the meridional section at 72.5°E and the zonal section at 65°S. (b–i) Vertical sections of potential temperature (color shading) with neutral density contours along 72.5°E (left column: b, d, f, h) and 65°S (right column: c, e, g, i) from April to July 2017. Black contours indicate neutral density (γ^n) in 2017, and magenta contours represent the 2010–2020 climatology (excluding 2017). The γ^n = 28.03 kg m^{-3} contours indicate the upper boundary of CDW.

3.2. Surface Forcing: Wind-Driven Divergence and Upwelling

The subsurface uplift described above coincided with anomalous atmospheric forcing over the study region. Previous work [He et al., 2024] identified anomalous Ekman pumping as an important trigger for the enhanced EKE during 2017. However, that analysis did not consider the potential role of sea-ice variability or the broader related processes operating across the regional system. Here, we revisit the atmospheric forcing within a broader air-ice-ocean context, examining how surface forcing anomalies interact with subsurface stratification and mesoscale dynamics. Beginning in March, wind anomalies developed over the continental slope region and northern open ocean, characterized by enhanced northward and northwestward wind components (Figure 3). By May, a pronounced cyclonic wind pattern was observed, associated with negative stress curl and enhanced Ekman upwelling along the continental slope. This upwelling weakened later in July and became less spatially coherent by August. The resulting Ekman divergence and associated transport favored the uplift of subsurface water masses. The temporal alignment supports a dynamical link between atmospheric forcing and interior ocean adjustment. Ekman-induced upwelling likely facilitated the shoreward intrusion of modified CDW near the continental slope (Figure 2), creating favorable conditions for subsequent mesoscale eddy activity and vertical exchanges.

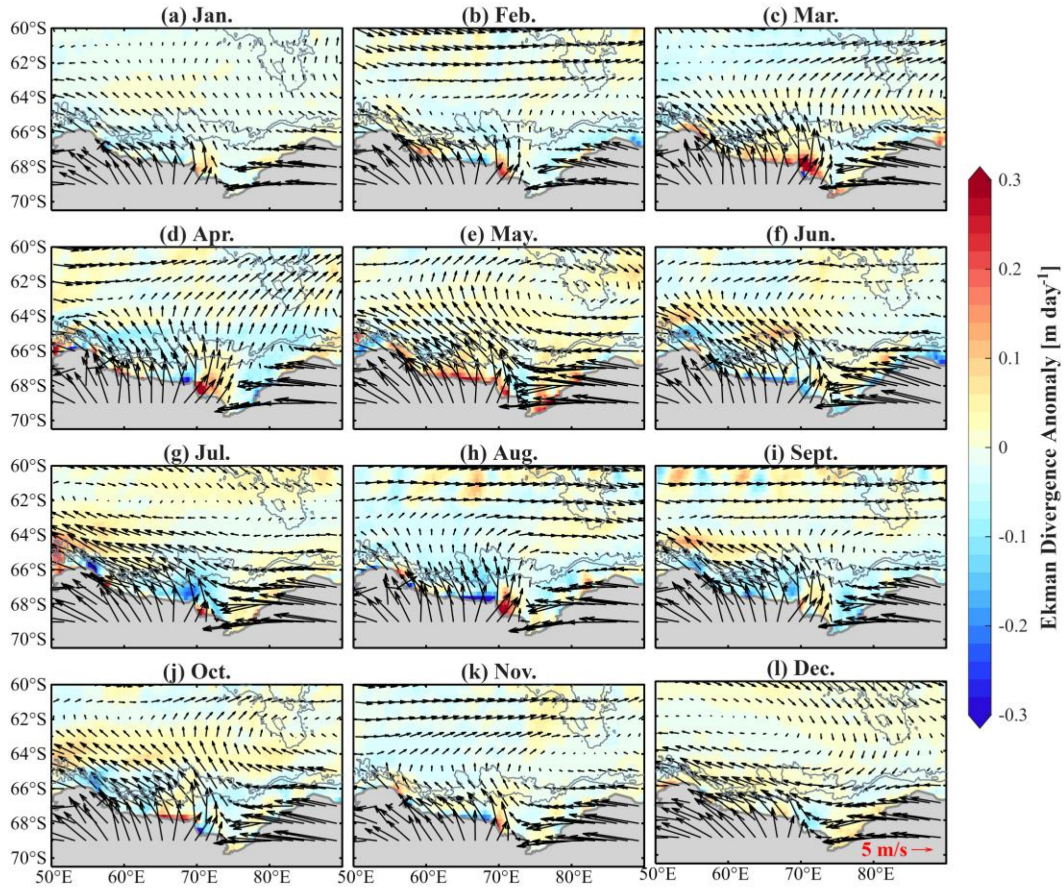

Figure 3. Monthly variations of 10-m wind vectors (arrows, m s^{-1}) and Ekman divergence anomalies (color shading, m day^{-1}) derived from surface stress including both wind and sea-ice contributions over the study region in 2017. Anomalies are relative to the monthly climatology. A reference vector of 5 m s^{-1} is shown in panel (l). Gray contours denote 2000 m and 3000 m isobaths.

3.3. Interior Ocean Response: Eddy Activity and Vertical Instability

To investigate the interior-ocean signature of the 2017 event, we analyzed meridional volume transport across 66°S, a section intersecting the convective region near Prydz Bay and lying just south of the most energetic eddy field, where cross-slope exchange is expected to influence the transport of warm water toward the bay (Figure 4). The transport integrated over 500–2000 m (Figure 4a) shows pronounced seasonal and interannual variability during 2010–2020, with the strongest anomaly in June 2017 (-5.8 Sv southward), the most intense poleward event within the analyzed record. Rather than implying a uniform zonal structure, Figures 4b-c show that the June 2017 circulation differs from the climatological mean by exhibiting stronger and more spatially organized zonal contrasts, with differences between the 60°–70°E and 70°–80°E sectors. In particular, the integrated southward signal is mainly contributed by the 70°–80°E region. The results thus provide the transport-based signature of the event, showing that the 2017 anomaly was associated with a strong intermediate-depth meridional circulation signal. We next examine the corresponding CDW-layer hydrographic anomalies to explore the water-mass conditions associated with that anomaly.

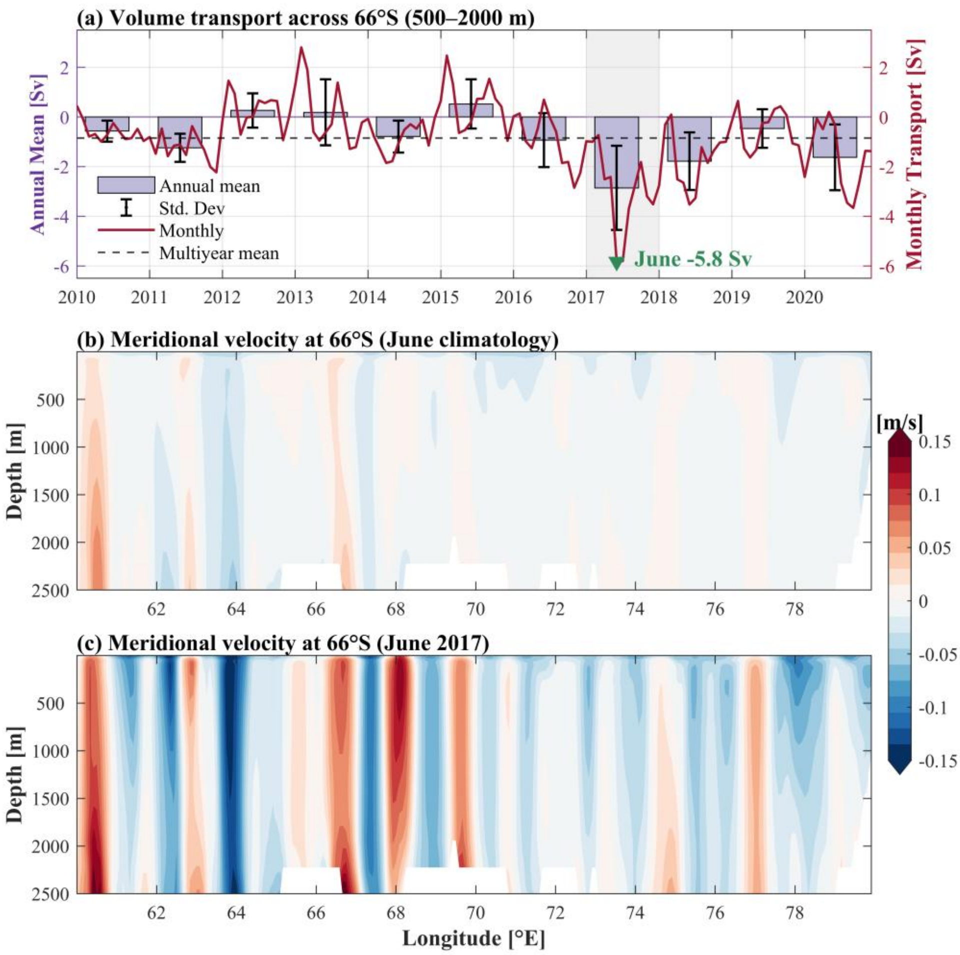

Figure 4. Meridional volume transport and velocity pattern across 66°. Volume transport is integrated across the transect between 60°E and 80°E. (a) Monthly (red line) and annual (purple bars) transport within a 500–2000 m depth range during 2010–2020. Black error bars denote the standard deviation of monthly values within each year, and the dashed line indicates the multiyear mean. The minimum (-5.8 Sv) occurred in June 2017 (green annotation). (b) Zonal distribution of meridional climatological velocity (m s^{-1}) at 66°S in June. (c) Same as (b), but for June 2017.

To characterize the variability of CDW, we isolated the neutral density range of $\gamma^n \approx 28.03$-28.27 kg m^{-3}, representative of the water-mass layer. Hydrographic anomalies during April-June 2017, relative to the climatology, indicate substantial modification of this layer over the southwestern Kerguelen Plateau and adjacent Prydz Bay sector (Figure 5), with temperature and salinity anomalies exceeding +0.3 °C and +0.05, respectively. These anomalies are pronounced across much of the 60°–80°E domain and suggest enhanced heat and salt transport, together with a lateral expansion of the CDW layer toward the continental slope, especially from April to July. This is consistent with the isopycnal shoaling and surface divergence described in Sections 3.1 and 3.2. The thickness of the CDW layer also expanded shoreward during winter (JAS).

Enhanced mesoscale activity accompanied these hydrographic changes (Figure 6). At CDW depths, the Rossby number ($Ro = \zeta/f$) exhibits marked increases from March to June, particularly over northern Prydz Bay, signaling intensified eddy activity (Figure 6a). A broad region of elevated EKE (> 300 cm^2 s^{-2}) develops on the eastern flank of the plateau (60°–80°E) (Figure 6b), co-located with persistent positive Ro anomalies (Ro > 0.06). In June, a dome-like isopycnal structure near 64°S, 73°E (Figures 2f, g) coincides with a localized Ro maximum, suggesting strong regional eddy activity. Although the Ro field appears spatially complex, the thermohaline sections (Figures 2 and S1) consistently show subsurface warming associated with uplifted isopycnals. These structures indicate shoreward intrusion and upward restructuring of warm CDW, bringing subsurface heat closer to the thermocline. Consistent with these hydrographic and mesoscale anomalies, the diagnosed convection depth (SCD) in June 2017 exceeds 2000 m near Prydz Bay (Figure 6c), which is deeper than the climatological range of approximately 700–1000 m and among the strongest values in the available record. The full monthly evolution of SCD is shown in the Supporting Information (Figure S2). This deep convection, likely associated with the combined effects of Ekman divergence and eddy-mediated vertical transport, points to weakened stratification and enhanced overturning. Together, these results suggest that mesoscale eddies and convection co-occur during the 2017 event, and that enhanced eddy-mean flow interaction and vertical energy redistribution contribute to both the deepening of convection and the upward restructuring of the CDW layer. We therefore next examine the underlying dynamical processes using energetics diagnostics.

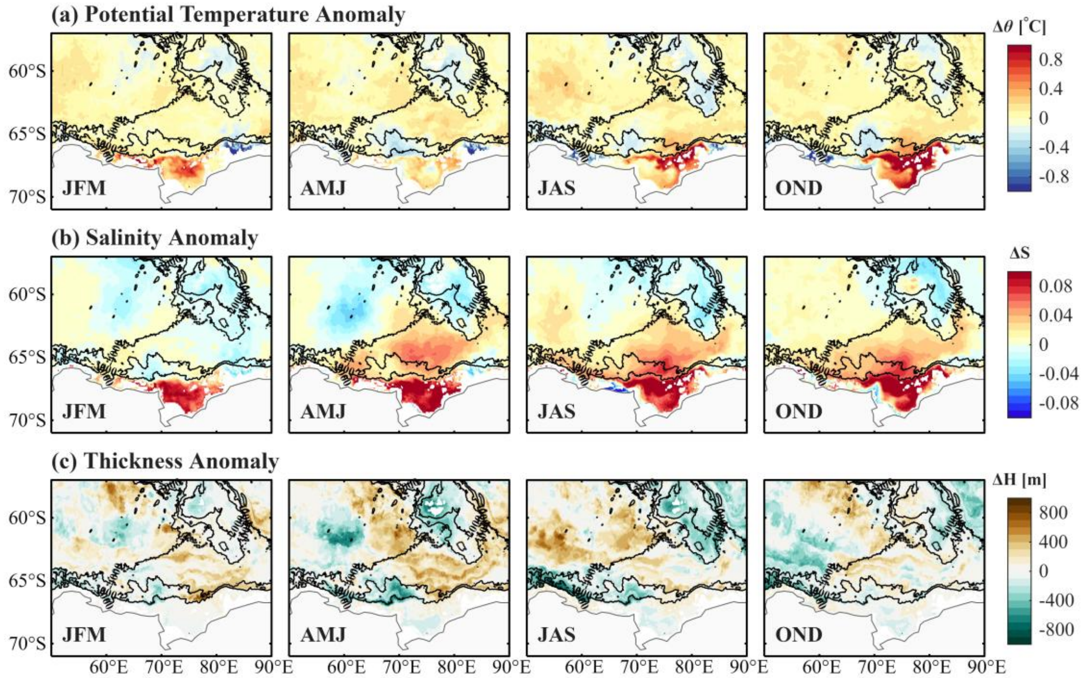

Figure 5. Seasonal anomalies of Circumpolar Deep Water (CDW) layer properties in 2017 relative to the 2010–2020 climatology (excluding 2017). Columns show anomalies of potential temperature (a), practical salinity (b), and thickness of CDW layer (c) of austral season: January–March (JFM), April–June (AMJ), July–September (JAS), and October–December (OND). The CDW layer is defined based on neutral density surfaces (γ_n). Black contours indicate isobaths with a contour interval of 1000 m.

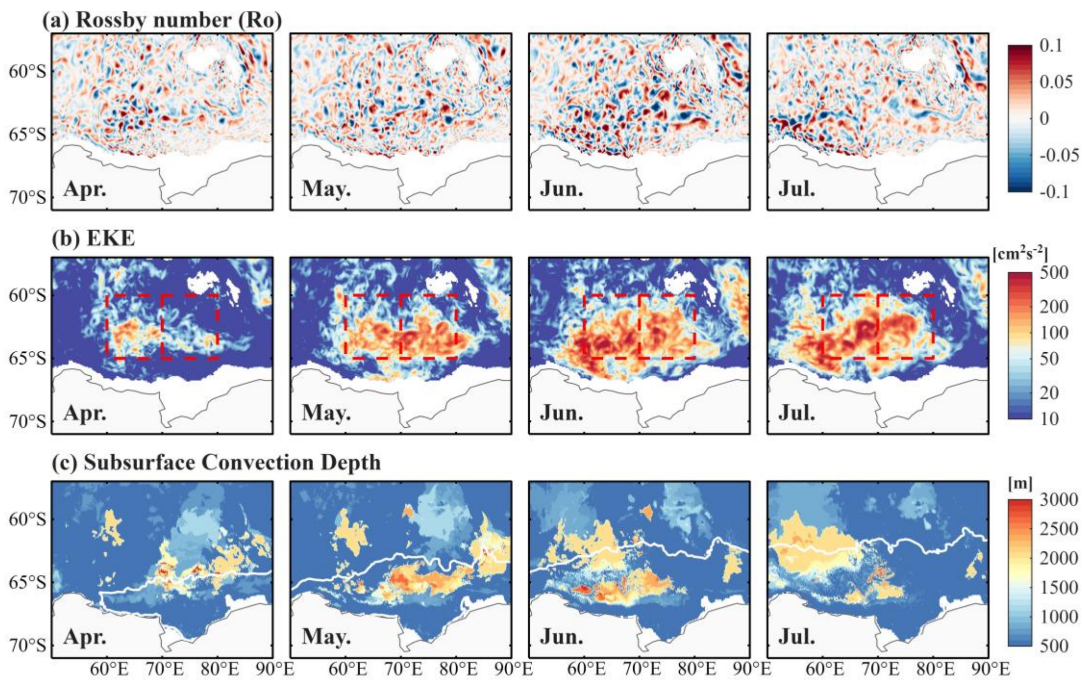

Figure 6. Monthly evolution of mesoscale dynamics and convective activity from March to June. (a) Rossby number (Ro) is calculated from relative vorticity at a depth of approximately 1500 m. (b) EKE at the same depth as Ro, displayed using a logarithmic (log10) color scale as Figure 1. Red dashed boxes indicate the region of enhanced mesoscale activity, and the area is divided zonally into two distinct sectors. (c) Subsurface Convection Depth (SCD) is defined by the maximum density gradient below 500 m, highlighting convection signals. White contours denote the 50% sea-ice concentration boundary.

3.4. Energy Conversion and Vertical Redistribution

The following analysis examines the vertical structure and regional contrasts of the energy pathways associated with the 2017 event, linking energy conversion more directly to the underlying processes and observed convective signals. In this framework, surface anomalies (Section 3.2) provide the relatively large-scale forcing that steepens isopycnals and preconditions the water column, while enhanced baroclinic conversion and eddy pressure-flux terms diagnosed here describe how the forcing is communicated into the subsurface and deeper layers.

Based on the spatial patterns of eddy activity shown in Figure 6, the energetics analysis focuses on two dynamically active longitude bands, 60°–70°E and 70°–80°E, which capture a strong contrast in baroclinic conversion and CDW-related overturning processes during the event. To investigate the distinct responses of these two regions, we conduct separate analyses of the regional energy budget and its vertical structure. Figure 7 compares the monthly variation of key energy components, and Figure 8 presents the corresponding energy conversion terms at representative depths. In the 70°–80°E sector, both MPE and EPE exhibit elevated values from March to June, particularly near 1000 m, consistent with the depth of the CDW core. Although both sectors show an increase in EKE during May-June, the 70°–80°E sector exhibits a substantially larger amplitude (Figures 7e–f), reflecting stronger eddy activity and enhanced release of potential energy through baroclinic processes. MKE shows a relatively steady enhancement from May to August in both sectors (Figures 7g–h), with slightly greater values in the 70°–80°E sector, likely reflecting strengthened currents modulated by local topography and seasonal atmospheric forcing.

The sectoral energy conversion analysis further clarifies the mechanisms driving this variability. In the 70°–80°E sector, baroclinic conversion (BCR: MPE → EPE) peaks sharply in May (Figure 8b), concentrated at 500–1000 m, indicating rapid release of potential energy stored in tilted isopycnals. This peak coincides with enhanced vertical eddy density flux (VEDF: EPE → EKE, Figure 8d), showing efficient conversion of potential energy into EKE in late autumn and supporting intensified eddy activity that promotes isopycnal deformation and upward restructuring of CDW. In contrast, the 60°–70°E sector shows weaker and more vertically confined BCR and VEDF signals (Figures 8a and 8c), implying relatively stable stratification. A localized BCR maximum near 2000 m suggests deep-layer instabilities, potentially associated with bottom-intensified shear linked to the DSW outflow along the continental slope. Barotropic conversion (BTR: MKE → EKE) remains comparatively small in both sectors (Figures 8e–f), although negative values in the eastern sector during autumn and winter imply episodes of energy transfer from eddies back to the mean flow, potentially modulating the slope current. Overall, these diagnostics (Figures 7 and 8) identify the 70°–80°E sector as the dominant region of baroclinic energy conversion during the event. Enhanced eddy activity across multiple depths in this region coincided with strong signals of CDW upwelling and deep convection. However, the conversion terms alone do not explain how the energy generated at depth is redistributed vertically to sustain the anomalous state. To address this question, the vertical structure of eddy energy fluxes is examined.

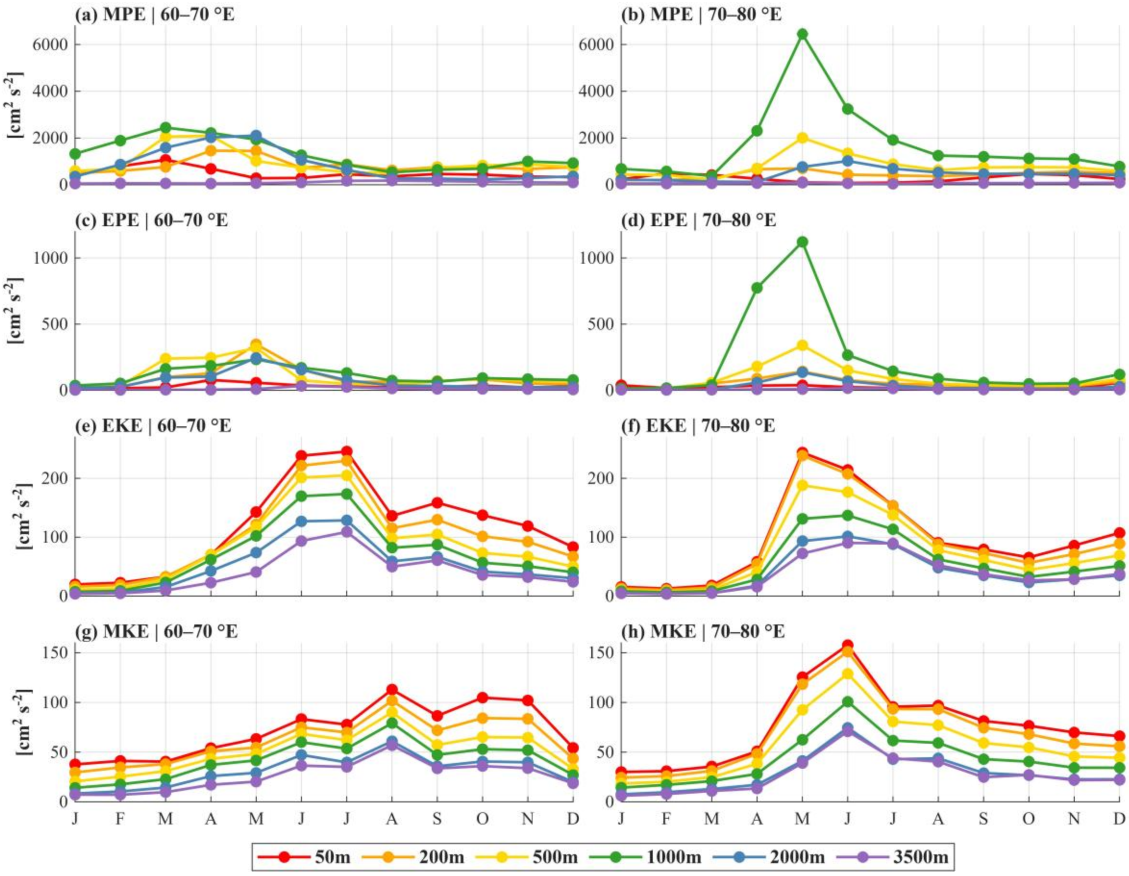

Figure 7. Monthly variations of energy components averaged over two sectors (60°–80°E) delineated by red dashed boxes in Figure 6: the 60°–70°E sector (left column) and the 70°–80°E sector (right column). Panels (a–b), (c–d), (e–f), and (g–h) illustrate mean potential energy (MPE), eddy potential energy (EPE), eddy kinetic energy (EKE), and mean kinetic energy (MKE), respectively. In each panel, curves denote time series at six representative depths: 50 m, 200 m, 500 m, 1000 m, 2000 m, and 3500 m.

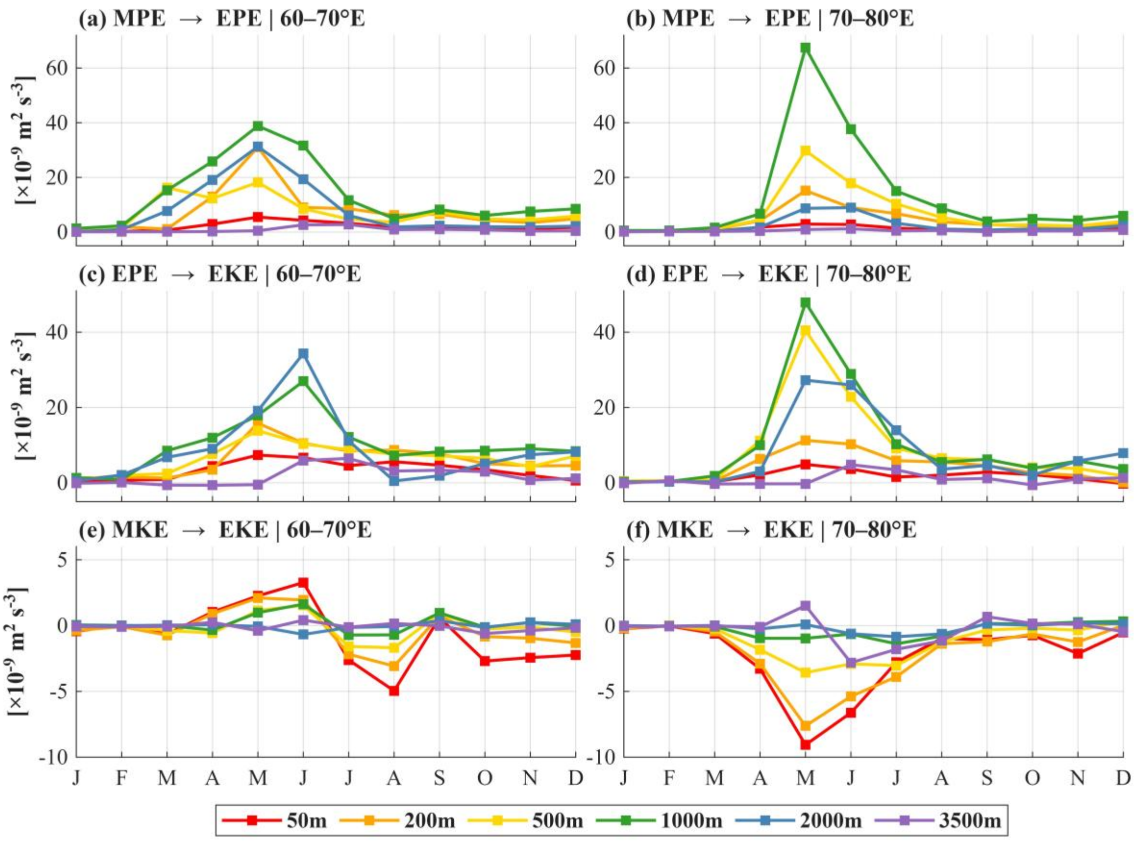

Figure 8. Monthly variations of energy conversion terms at representative depths for the two selected sectors, same as Figure 7. Panels (a–b): baroclinic conversion (BCR: MPE → EPE); (c–d): vertical eddy density flux (VEDF: EPE → EKE), which indicates eddy generation directly; (e–f): barotropic conversion (BTR: MKE → EKE).

Vertical distributions of eddy energy flux components from April to July 2017 for the two sectors are analyzed (Figures 9 and 10). In the 70°–80°E sector (Figure 9), strong vertical eddy density flux (VEDF) is evident in May, centered between 500 and 1500 m, coinciding with the depth range of the CDW core. This signal is accompanied by negative vertical pressure-flux divergence (Figure 9c) within the depth range at around 1000 m, indicating convergence of eddy energy into this layer. This convergence suggests an accumulation of energy at intermediate depths, which may support enhanced convective activity. The horizontal pressure-flux divergence (Figure 9b) shows lateral energy redistribution that is dynamically linked to the vertical energy exchange. The 60°–70°E sector (Figure 10) displays a different vertical structure. Here, the strongest VEDF signals occur closer to the continental slope, with a deeper and more localized enhancement in June (Figure 10a), likely associated with DSW export. The vertical pressure-flux convergence (negative values) in this region is distributed at greater depths than those in the 70°–80°E sector, closer to the depth range of the outflow. These results reinforce the earlier interpretation that the 70°–80°E sector is dynamically more active, exhibiting stronger eddy-driven vertical energy redistribution within the CDW layer, whereas the 60°–70°E domain is dominated by more localized, bottom-intensified processes associated with DSW export. Although the EKE advection term was also examined, it is characterized by localized positive and negative anomalies and does not show a coherent structure associated with CDW intrusion or deep convection. Therefore, our discussion focuses on the pressure-work term, which provides a clearer diagnosis of vertical eddy energy redistribution during the 2017 event.

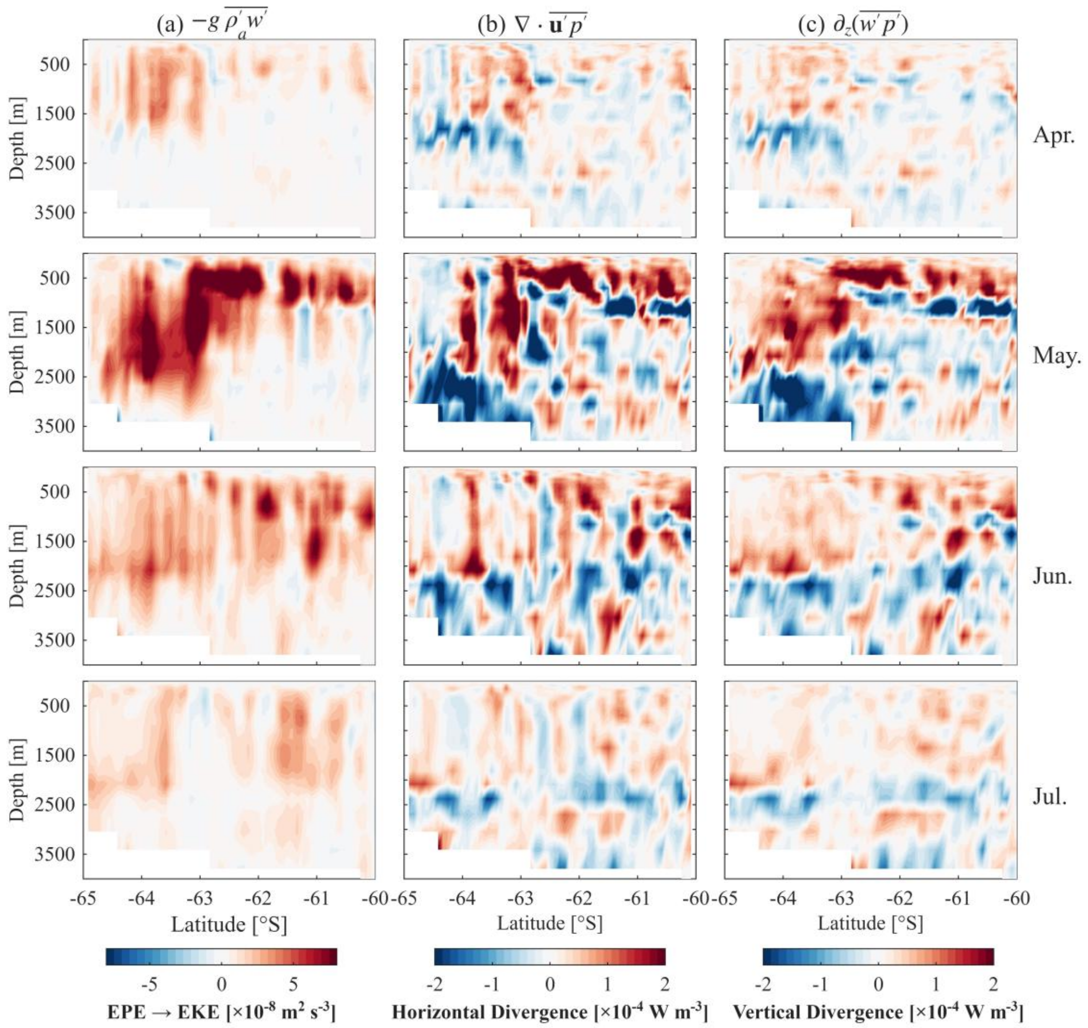

Figure 9. Vertical distributions of eddy energy flux components from April to July 2017, zonally averaged over the 70°–80°E sector, adjacent to Prydz Bay, where eddy activity and

514 CDW upwelling are more prominent. (a) Vertical eddy density flux (VEDF, $-g\overline{\rho_a{}'w'}$),
515 representing the conversion from eddy potential energy to eddy kinetic energy (EPE → EKE).
516 (b) Horizontal eddy pressure-flux divergence ($\nabla \cdot \overline{\boldsymbol{u}'p'}$), and (c) the vertical derivative of the
517 vertical eddy pressure-flux ($\partial_z \overline{w'p'}$), both indicating redistribution of eddy energy. Positive
518 values (warm colors) represent energy divergence, while negative values (cool colors)
519 indicate energy convergence. Units are 10^{-8} m^{2}s^{-3} for VEDF and 10^{-4} W m^{-3} for the
520 pressure-flux divergence terms.
521

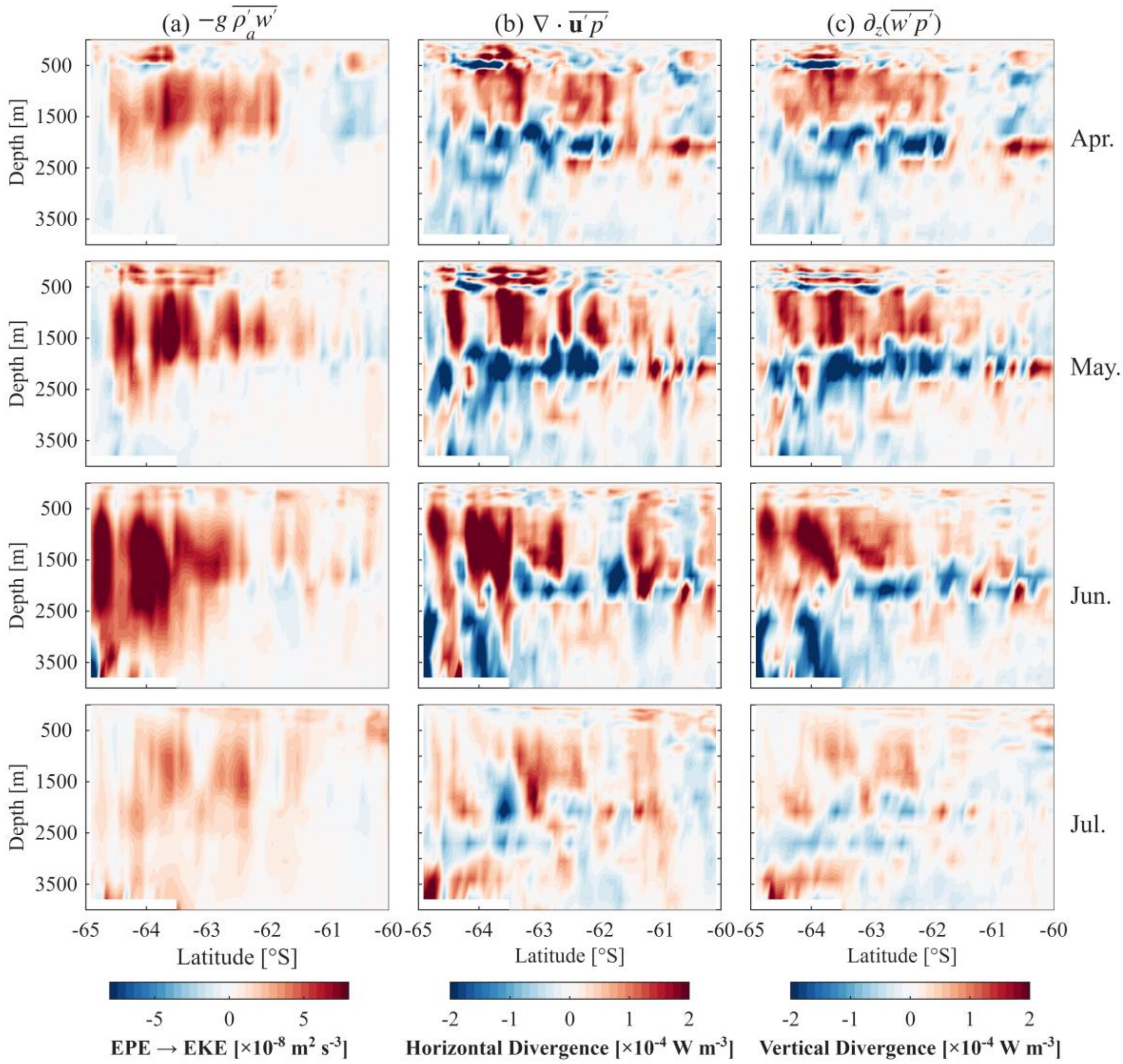

522 **Figure 10.** Same as Figure 9, but for the 60°–70°E sector.

523 **3.5. Volume-Heat Transport Asymmetry and Eddy Contributions**

While Section 3.4 diagnosed the energetic pathways responsible for mesoscale variability, this section examines how these dynamical processes are reflected in regional circulation and property fluxes. To place the Prydz Bay anomaly in a broader regional context, we extend the analysis here to three longitude bands: 50°–60°E, 60°–70°E, and 70°–80°E. This comparison highlights the zonal asymmetry of circulation and property fluxes. The mechanistic analysis of eddies and convection in the previous section remains focused on the 60°–80°E region, while the additional western band provides context for the broader spatial structure. Meridional volume transports across these sectors are analyzed to identify depth-dependent and zonally asymmetric patterns (Figure 11).

Consistent with the poleward transport anomaly within the CDW layer identified in Figure 4, the expanded sector analysis reveals clear zonal contrasts in transport structure. The 70°–80°E sector (Figure 11c) is dominated by persistent southward transport within both the upper (0–500 m) and intermediate (500–2000 m) layers, indicating sustained inflow of relatively warm water toward the slope. The intermediate layer shows a particularly strong southward anomaly in June (Figure 4a), the strongest in the 11-year record. In contrast, the 50°–60°E sector (Figure 11a) shows northward transport across all depth ranges, consistent with export of dense shelf water away from the continental margin. At depths greater than 500 m, the 50°–60°E sector shows persistent northward transport after April that reinforces its role as a pathway for water export. The 60°–70°E sector between these two (Figure 11b) exhibits weaker and more variable transport signals, suggesting that it acts as a transitional zone between the DSW-dominated outflow regime in the west and the CDW-inflow regime in the east. Together, these zonal differences reveal an asymmetric overturning structure: CDW inflow dominates the 70°–80°E sector, while northward export of dense water is most evident in the 50°–60°E sector. These contrasting volume transports provide the dynamical context for the subsequent analysis of heat fluxes (Figures 12 and 13), highlighting the interplay between mean flows and eddy activity in shaping vertical heat redistribution.

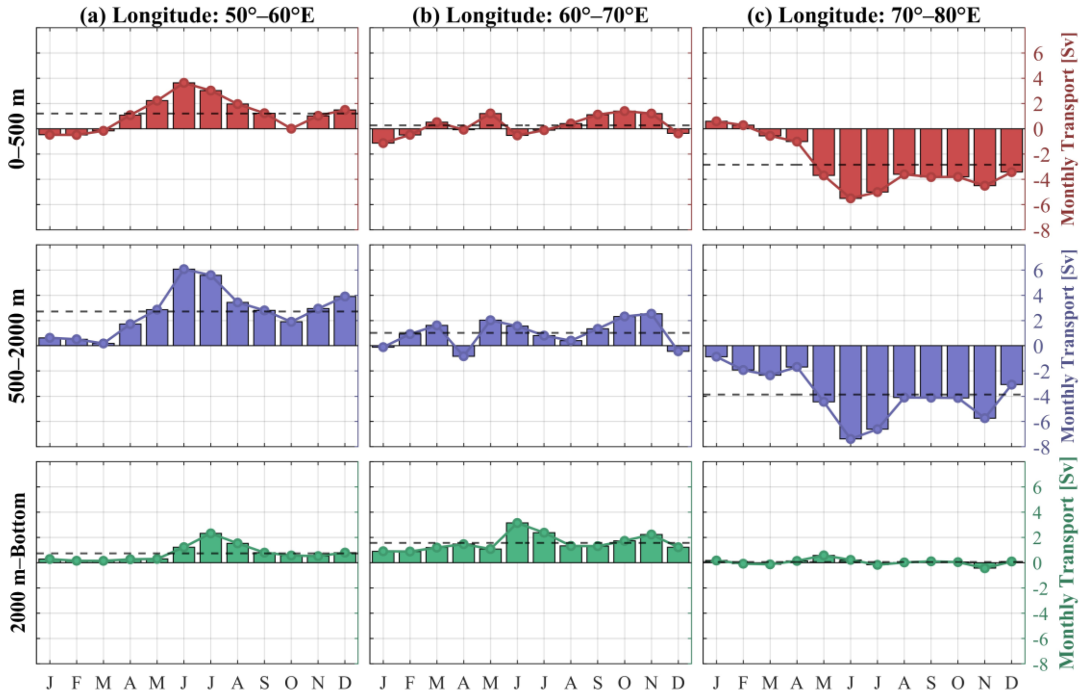

Figure 11. Monthly meridional volume transport in 2017 across three longitude sectors: (a) 50°–60°E, (b) 60°–70°E, and (c) 70°–80°E. Each panel shows transport integrated over three depth ranges: 0–500 m, 500–2000 m, and 2000 m–bottom. Positive values indicate northward transport, and negative values indicate southward (poleward) transport. Dashed horizontal lines denote the annual mean for each depth range.

Monthly mean and eddy components of regional heat flux are separated to characterize vertical and temporal variability to further explore how the observed recirculation affects property exchange (Figures 12 and 13). In the upper ocean (0–1000 m), southward heat flux dominates during austral summer and autumn. This pattern coincides with periods of intensified Ekman divergence (Figure 2) and surface heat loss, indicating that surface forcing and Ekman-driven upwelling jointly modulate the upper-ocean heat distribution during the preconditioning phase. At intermediate depths, the heat flux becomes more regionally distinct (Figure 12). The eastern 70°–80°E sector shows intermittent signals, with occasional southward pulses that suggest CDW inflow but limited vertical coupling. In contrast, in the western 50°–60°E sector, persistent negative heat flux values appear during autumn and winter (from April), reflecting the northward export of cold, dense water, which in heat-flux terms is equivalent to a southward transport of heat. This signal is consistent with localized activity and dense water export, underscoring its role in ventilating the abyss as a key site of AABW export.

The central 60°–70°E sector shows weaker and more variable signals, reinforcing its role as a transitional region between the two regimes. Figure 13 isolates the eddy-driven component of heat transport, highlighting the contribution of transient eddies in redistributing heat within the water column. Eddy heat convergence intensifies below ~500 m between April and June, with a maximum in May, especially in the 70°–80°E sector. This timing and depth range coincide with enhanced vertical energy conversion diagnosed in Figures 9 and 10, confirming that mesoscale eddies play a key role in redistributing heat upward from the CDW layer into the mid-depth ocean during the 2017 event.

Overall, these results suggest a coherent mechanism in which anomalous surface forcing induces upper-ocean divergence and stratification preconditioning, followed by intensified mesoscale eddy activity and enhanced eddy-mean flow interactions that drive vertical energy redistribution. These processes facilitate deep convection and the uplift of CDW. The proposed mechanism and its vertical structure are synthesized schematically in Figure 14.

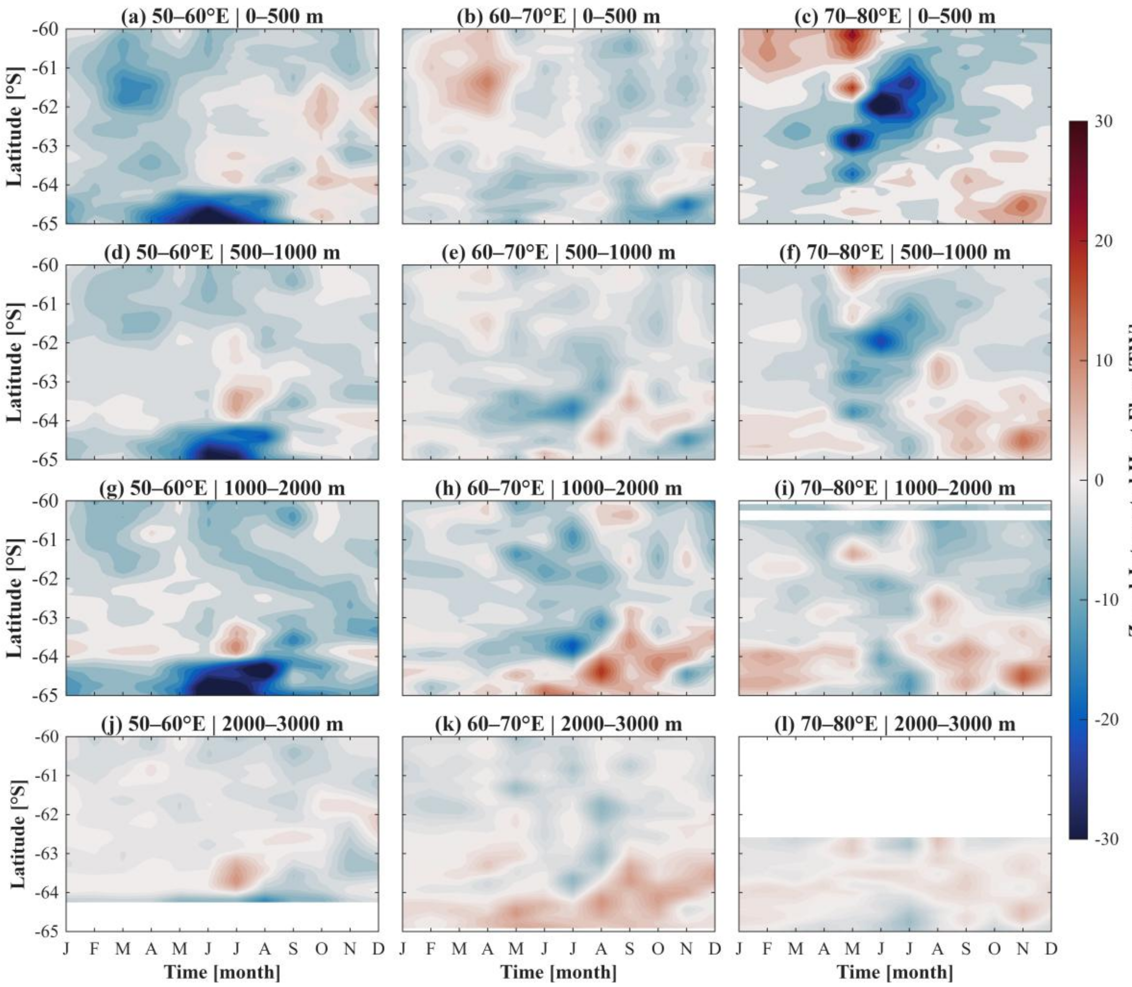

Figure 12. Hovmöller diagrams of zonally integrated monthly mean ocean heat flux (TW) in three sectors adjacent to Prydz Bay in 2017: (a, d, g, j) 50°–60°E, (b, e, h, k) 60°–70°E, and (c, f, i, l) 70°–80°E, computed relative to a reference temperature of 0 °C. Each panel shows depth-integrated values over a specific depth interval: (a–c) 0–500 m, (d–f) 500–1000 m, (g–i) 1000–2000 m, and (j–l) 2000–3000 m. Negative values indicate southward transport; in the 50°–60°E sector, these values also reflect the northward export of cold, dense water in the regional heat budget. White areas denote masked regions without valid data due to bathymetric constraints.

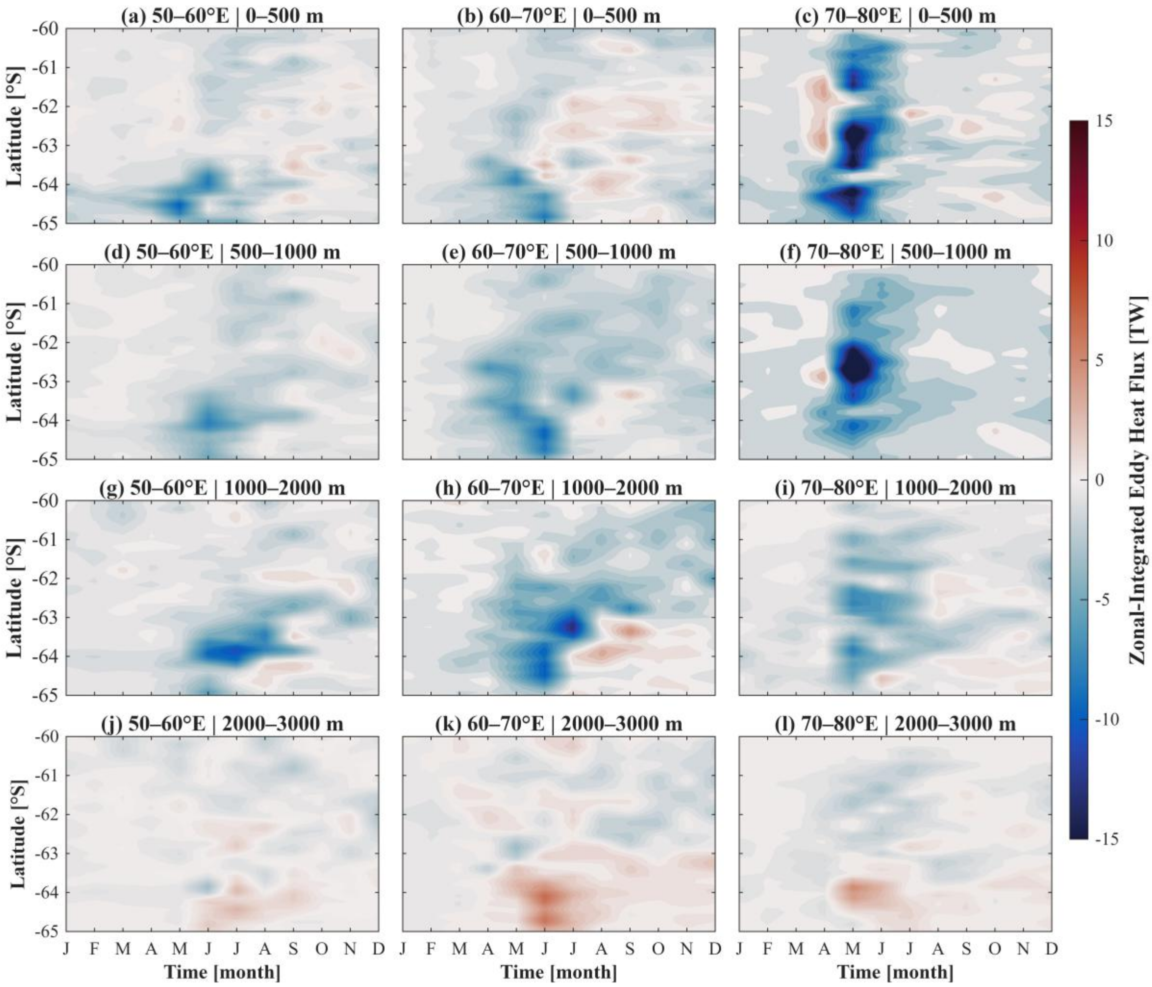

Figure 13. Hovmöller diagrams of zonally integrated meridional eddy heat flux over the same regions and depth intervals as in Figure 12. Eddy fluxes are derived from daily anomalies and are independent of the reference temperature.

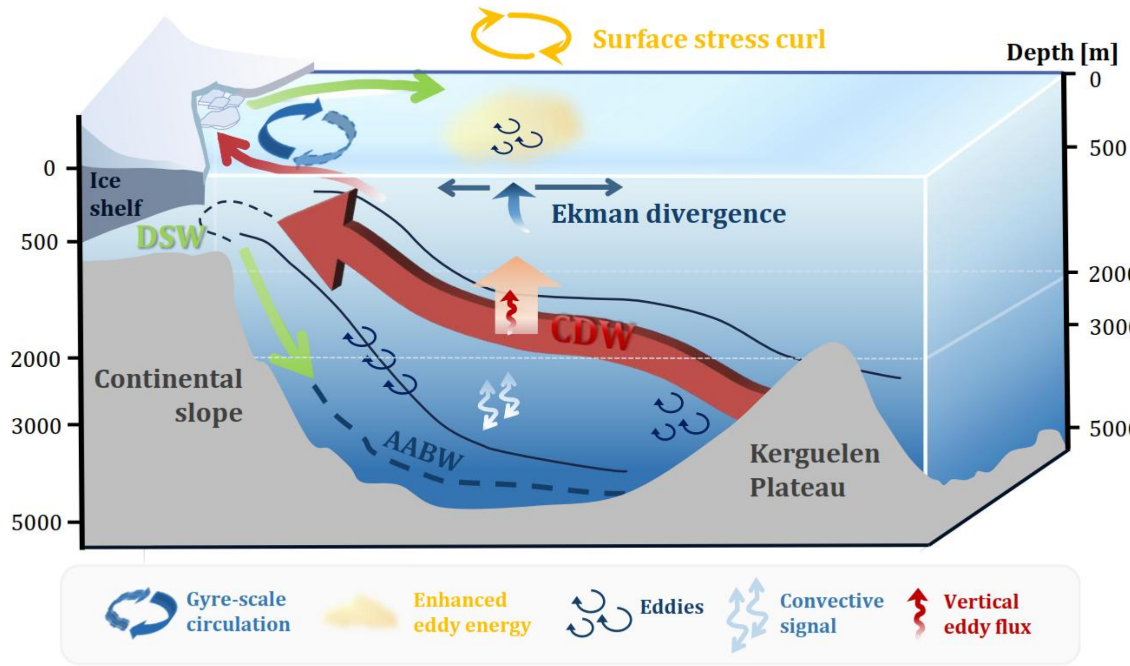

Figure 14. Schematic summary of the processes associated with the 2017 deep-convection event in the study region. Anomalous surface stress pattern induces Ekman divergence near the continental slope, promoting upward displacement of subsurface water masses. This surface forcing preconditions the upper ocean by steepening isopycnals. Concurrently, enhanced mesoscale eddy activity intensifies baroclinic energy conversion and strengthens vertical eddy heat fluxes within the CDW layer. The resulting vertical energy redistribution, with eddy-driven mixing, facilitates the uplift of CDW and further weakens stratification, enabling convection to extend to depths exceeding 2000 m. The combined effects of surface forcing, eddy energetics, and vertical exchange sustain an anomalous regional circulation, characterized by CDW inflow along the slope and shelf water export, forming a zonally asymmetric overturning structure influenced by regional bathymetry.

4. Discussion

This study highlights a dynamically coupled set of processes that contributed to the anomalously strong deep convection observed in the Cooperation Sea and adjacent Prydz Bay region during the austral autumn-winter of 2017 (summarized schematically in Figure 14). By integrating diagnostics of surface forcing, eddy energetics, and vertical heat redistribution, we present a framework showing how transient atmospheric perturbations propagate downward, interact with enhanced mesoscale activity, sustain vertical exchange, and enable deep convection.

Although the event was initially triggered by anomalous atmospheric forcing that enhanced Ekman divergence, our diagnostics show that mesoscale eddies played a key role in sustaining vertical exchange and enabling deep convection. Enhanced baroclinic conversion and vertical eddy density fluxes during May–June indicate that eddies actively intensified buoyancy transfer and weakened stratification, enabling convection to extend well below 2000 m despite surface freshening and record-low sea ice [Wang et al., 2019; Sabu et al., 2021]. Persistent deep convective signals suggest a dynamically coupled wind-eddy-convection mode of variability. Jüling et al. [2018] showed that multidecadal Southern Ocean variability, termed the Southern Ocean Mode, emerges through a Lorenz-energy-cycle pathway in which wind work on the mean flow steepens isopycnals, baroclinic conversion energizes eddies, and deep convection coincides with enhanced eddy activity, surface warming, and release of deep heat. The energetics diagnosed here confirm that the anomaly in 2017 may represent a regional example of this Southern Ocean mode, with local topography (e.g., the Kerguelen Plateau and downstream troughs) shaping regional patterns of CDW inflow and DSW outflow.

The sector-resolved flux analysis reveals a clear zonal asymmetry: persistent southward CDW inflow in the east and northward DSW export in the west. This configuration resembles a coupled overturning cell in which eddy-mediated inflow balances shelf-driven outflow. Comparable structures have been described in the Ross Sea, where troughs along the continental shelf support DSW export on one side and CDW inflow on the other [Lanham et al., 2025]. Jendersie et al. [2018] further showed that Ross Sea circulation intensifies in winter through density forcing and shelf-slope interaction, demonstrating that buoyancy-driven processes can couple with wind and eddy dynamics. Similarly, in the Amundsen and Bellingshausen Seas, Nakayama et al. [2018] found that large-scale circulation and boundary water properties control CDW pathways and shelf intrusions. Our findings extend these results to Prydz Bay, showing how regional bathymetry projects large-scale modes onto a zonally confined recirculation system. A novel aspect of this study is the simultaneous identification of both overturning branches across the Prydz Bay region during this anomalous year.

The 2017 anomalies may thus reflect both transient surface forcing and broader shifts in Southern Ocean circulation. While such processes are consistent with emerging Southern Ocean modes, the magnitude of the 2017 event was unusually strong within the available record. In the depth range of CDW, volume transport showed a record southward anomaly, and convection extended to depths exceeding 2000 m, substantially deeper than the climatological mean. These characteristics raise the question of whether the event was expected under ongoing climate trends or represents a rare outlier. Freshwater input has long been recognized to enhance upper-ocean stratification and inhibit deep-water formation in the Southern Ocean [Richardson et al., 2005; Swingedouw et al., 2009]. More recently, Li et al. [2023] suggested that increased Antarctic meltwater fluxes further freshen the surface ocean, strengthen upper-ocean stratification, and suppress the formation of AABW, thereby slowing abyssal overturning. The anomalies observed in 2017 challenge this expectation, suggesting either an exceptional departure from typical conditions or the influence of concurrent processes, such as surface salinification and reduced sea ice cover, that temporarily weakened stratification and allowed deep convection to occur.

Recent observations suggest that the Southern Ocean may be entering a new stratification regime. Silvano et al. [2025] reported a widespread and abrupt increase in surface salinity across the Southern Ocean since 2015, reversing decades of freshening and coinciding with record-low sea ice. This salinification weakened the upper-ocean stratification, favoring vertical heat exchange and the reemergence of open-ocean polynyas. Purich and Doddridge [2023] likewise point to a shift in ice-ocean interactions toward a new state. Our findings expand on this emerging view. We show that the event cannot be explained by surface anomalies alone; rather, it likely reflects the interaction of this forcing with a pre-existing weakened stratification. This interaction likely increased the ocean’s sensitivity, combined with the vertical extension of eddy activity reaching over 2000 m. It facilitated the extreme overturning event. Taken together, the results indicate that although long-term warming generally suppresses deep convection, episodic events such as those in 2017, perhaps when wind stress, sea ice retreat, and local bathymetry align, could act as triggers, indicating that threshold controlling vertical exchange may be more variable and potentially lower than assumed in many current models. The Southern Ocean may become more prone to deep convection events, with profound implications for the formation of AABW, ventilation of deep carbon reservoirs, and global heat redistribution [Heywood et al., 2014; Silvano et al., 2023; Blanckensee et al., 2024].

Collectively, our results support a framework in which surface stress-driven divergence and deep eddy-induced convergence jointly regulate the timing, depth, and intensity of convection. This coupling governs CDW and DSW pathways, shapes local recirculation, and links surface forcing with deep overturning. The 2017 event thus provides rare evidence that extreme wind and eddy perturbations can overcome stratification thresholds. Sustained observations (e.g., mooring arrays and Biogeochemical-Argo floats) together with eddy-resolving models will be essential to test whether the linkage diagnosed here is systematically triggered under climate change.

5. Conclusions

In this study, we applied an energetics-based diagnostic framework to the 2017 deep-convection anomaly off Prydz Bay and identified a coherent mechanism linking surface forcing to deep-ocean responses (Figure 14). Analyses of neutral density structure, energy conversions, and vertical eddy energy fluxes indicate that intensified mesoscale eddy activity, together with changes in stratification, contributed to sustaining the deep overturning observed during the event. This case illustrates how eddy-mean flow interactions can sustain a surface-to-depth response that involves both atmospheric forcing and internal ocean dynamics. Surface forcing anomalies induce Ekman divergence and modify upper-ocean stratification, while enhanced eddy-mean flow interactions promote baroclinic energy conversion and vertical eddy energy fluxes within the CDW layer. These processes sustain vertical exchanges that propagate the signal into the deep ocean and modulate interior heat redistribution. Our results highlight the role of mesoscale energy pathways in regulating vertical exchange in the subpolar ocean, a process that remains unresolved in coarse-resolution climate models. Consequently, although Earth system models are sensitive to deep convection in the Southern Ocean, they may not fully capture the mesoscale processes described here and may therefore underestimate the sensitivity of overturning variability to atmospheric forcing. Further observations and high-resolution simulations are needed to evaluate the recurrence, spatial variability, and climatic impacts of such self-amplifying events. Understanding these mechanisms is essential for improving projections of Southern Ocean overturning and its role in global climate regulation.

Data Availability Statement

The oceanic reanalysis product used in this study is obtained from the Copernicus Marine Environmental Monitoring Service (CMEMS) GLORYS12V1 product (GLOBAL_REANALYSIS_PHY_001_030) available at: https://data.marine.copernicus.eu/product/GLOBAL_MULTIYEAR_PHY_001_030/services. Atmospheric forcing fields are derived from the ERA5 reanalysis provided by the European Center for Medium-Range Weather Forecasting (ECMWF) interim reanalysis dataset (https://cds.climate.copernicus.eu/datasets/reanalysis-era5-single-levels-monthly-means?tab=download). The bathymetry is provided by the ETOPO 2022 15 Arc-Second Global Relief Model available through the NOAA National Centers for Environmental Information (2022) (https://www.ncei.noaa.gov/products/etopo-global-relief-model). The figures are created with software MATLAB R2022a (The MathWorks, Inc, 2022; https://www.mathworks.com/).

Conflict of Interest Statement

The authors declare no conflicts of interest relevant to this study.

Acknowledgments

This work is supported by the Natural Science Foundation of China (Grant 41941008), the Ministry of Natural Resources of the People's Republic of China (Grant 583 No: IRASCC 1-02-01B), the Shanghai Frontiers Science Center of Polar Science (SCOPS), and Shanghai Key Laboratory of Polar Life and Environment Sciences (Grant 21DZ2260100). Y. He acknowledges support from the China Scholarship Council (CSC). The authors sincerely appreciate the editor and the reviewers for their constructive comments, careful assessment, and valuable suggestions throughout the review process.

References

Blanckensee, S. N., D. E. Gwyther, B. K. Galton-Fenzi, K. L. Gunn, L. Herraiz-Borreguero, K. I. Ohshima, E. Portela, A. L. Post, and H. C. Bostock (2024), A Review of the Oceanography and Antarctic Bottom Water Formation Offshore Cape Darnley, East Antarctica, *Journal of Geophysical Research: Oceans*, *129*(10), e2024JC021251, doi:https://doi.org/10.1029/2024JC021251.

Comiso, J. C., D. J. Cavalieri, and T. Markus (2003), Sea ice concentration, ice temperature, and snow depth using AMSR-E data, *IEEE Transactions on Geoscience and Remote Sensing*, *41*(2), 243-252, doi:10.1109/TGRS.2002.808317.

Gao, L., X. Yuan, W. Cai, G. Guo, W. Yu, J. Shi, F. Qiao, Z. Wei, and G. D. Williams (2024), Persistent warm-eddy transport to Antarctic ice shelves driven by enhanced summer westerlies, *Nature Communications*, *15*(1), doi:10.1038/s41467-024-45010-x.

Guo, G., L. Gao, J. Shi, and Y. Zu (2022), Wind-Driven Seasonal Intrusion of Modified Circumpolar Deep Water Onto the Continental Shelf in Prydz Bay, East Antarctica, *Journal of Geophysical Research: Oceans*, *127*(12), doi:10.1029/2022jc018741.

Guo, G., J. Shi, L. Gao, T. Tamura, and G. D. Williams (2019), Reduced Sea Ice Production Due to Upwelled Oceanic Heat Flux in Prydz Bay, East Antarctica, *Geophysical Research Letters*, *46*(9), 4782-4789, doi:10.1029/2018gl081463.

He, Q., W. Zhan, S. Cai, Y. Du, Z. Chen, S. Tang, and H. Zhan (2023), Enhancing impacts of mesoscale eddies on Southern Ocean temperature variability and extremes, *Proceedings of the National Academy of Sciences of the United States of America*, *120*(39), e2302292120-e2302292120, doi:10.1073/pnas.2302292120.

He, Y., M. Zhou, and D. Kang (2024), Strong Eddy Kinetic Energy Anomalies Induced by Baroclinic Instability in the Southwest Region of the Kerguelen Plateau, East Antarctica, *Journal of Geophysical Research: Oceans*, *129*(6), doi:10.1029/2023JCO20667.

Heywood, K. J., et al. (2014), Ocean processes at the Antarctic continental slope, *Philosophical Transactions of the Royal Society a-Mathematical Physical and Engineering Sciences*, *372*(2019), doi:10.1098/rsta.2013.0047.

Jendersie, S., M. J. M. Williams, P. J. Langhorne, and R. Robertson (2018), The Density-Driven Winter Intensification of the Ross Sea Circulation, 123(11), 7702-7724, doi:https://doi.org/10.1029/2018JC013965.

Jüling, A., J. P. Viebahn, S. S. Drijfhout, and H. A. Dijkstra (2018), Energetics of the Southern Ocean Mode, *Journal of Geophysical Research: Oceans*, *123*(12), 9283-9304, doi:10.1029/2018jc014191.

Kang, D., and E. N. Curchitser (2015), Energetics of Eddy-Mean Flow Interactions in the Gulf Stream Region, *Journal of Physical Oceanography*, *45*(4), 1103-1120, doi:10.1175/jpo-d-14-0200.1.

Kang, D., and E. N. Curchitser (2017), On the Evaluation of Seasonal Variability of the Ocean Kinetic Energy, *Journal of Physical Oceanography*, *47*(7), 1675-1683, doi:10.1175/jpo-d-17-0063.1.

Li, Q., M. H. England, A. M. Hogg, S. R. Rintoul, and A. K. Morrison (2023), Abyssal ocean overturning slowdown and warming driven by Antarctic meltwater, *Nature*, *615*(7954), 841-847, doi:10.1038/s41586-023-05762-w.

Liu, C., Z. Wang, C. Cheng, R. Xia, B. Li, and Z. Xie (2017), Modeling modified Circumpolar Deep Water intrusions onto the Prydz Bay continental shelf, East Antarctica, *Journal of Geophysical Research: Oceans*, *122*(7), 5198-5217, doi:10.1002/2016jc012336.

Matsuta, T., and Y. Masumoto (2023), Energetics of the Antarctic Circumpolar Current. Part I: The Lorenz Energy Cycle and the Vertical Energy Redistribution, *Journal of Physical Oceanography*, *53*(6), 1467-1484, doi:10.1175/jpo-d-22-0133.1.

McKee, D. C., D. G. Martinson, and O. Schofield (2019), Origin and Attenuation of Mesoscale Structure in Circumpolar Deep Water Intrusions to an Antarctic Shelf, *Journal of Physical Oceanography*, *49*(5), 1293-1318, doi:10.1175/jpo-d-18-0133.1.

Meijers, A. J. S., A. Klocker, N. L. Bindoff, G. D. Williams, and S. J. Marsland (2010), The circulation and water masses of the Antarctic shelf and continental slope between 30 and, *Deep Sea Research Part II: Topical Studies in Oceanography*, *57*(9-10), 723-737, doi:10.1016/j.dsr2.2009.04.019.

Meehl, G. A., J. M. Arblaster, C. T. Y. Chung, M. M. Holland, A. DuVivier, L. Thompson, D. Yang, and C. M. Bitz (2019), Sustained ocean changes contributed to sudden Antarctic sea ice retreat in late 2016, *Nature Communications*, *10*, doi:10.1038/s41467-018-07865-9.

Morrison, A. K., A. M. Hogg, M. H. England, and P. Spence (2020), Warm Circumpolar Deep Water transport toward Antarctica driven by local dense water export in canyons, *Science Advances*, *6*(18), eaav2516, doi:doi:10.1126/sciadv.aav2516.

Nakayama, Y., D. Menemenlis, H. Zhang, M. Schodlok, and E. Rignot (2018), Origin of Circumpolar Deep Water intruding onto the Amundsen and Bellingshausen Sea continental shelves, Nat Commun, 9(1), 3403, doi:10.1038/s41467-018-05813-1.

Nøst, O. A., M. Biuw, V. Tverberg, C. Lydersen, T. Hattermann, Q. Zhou, L. H. Smedsrud, and K. M. Kovacs (2011), Eddy overturning of the Antarctic Slope Front controls glacial melting in the Eastern Weddell Sea, *Journal of Geophysical Research: Oceans*, *116*(C11), doi:10.1029/2011jc006965.

Nunes Vaz, R. A., and G. W. Lennon (1996), Physical oceanography of the Prydz Bay region of Antarctic waters, *Deep-Sea Research Part I: Oceanographic Research Papers*, *43*(5), 603-641, doi:10.1016/0967-0637(96)00028-3.

Oelerich, R., K. J. Heywood, G. M. Damerell, and A. F. Thompson (2022), Wind-Induced variability of warm water on the southern Bellingshausen Sea continental shelf, *Journal of Geophysical Research: Oceans*, *127*(11), e2022JC018636, doi:https://doi.org/10.1029/2022JC018636.

Ohshima, K. I., et al. (2013), Antarctic BottomWater production by intense sea-ice formation in the Cape Darnley polynya, *Nature Geoscience*, *6*(3), 235-240, doi:10.1038/ngeo1738.

Orsi, A., W. Thomas, and W. D. Nowlin (1995), On the meridional extent and fronts of the Antarctic Circumpolar Current, *Deep Sea Research Part I: Oceanographic Research Papers*.

Park, Y.-H., et al. (2019), Observations of the Antarctic Circumpolar Current over the Udintsev Fracture Zone, the narrowest choke point in the Southern Ocean, *Journal of Geophysical Research: Oceans*, *124*(7), 4511-4528, doi:https://doi.org/10.1029/2019JC015024.

Purich, A., and E. W. Doddridge (2023), Record low Antarctic sea ice coverage indicates a new sea ice state, Communications Earth & Environment, 4(1), 314, doi:10.1038/s43247-023-00961-9.

Richardson, G., M. R. Wadley, K. J. Heywood, D. P. Stevens, and H. T. Banks (2005), Short-term climate response to a freshwater pulse in the Southern Ocean, Geophysical Research Letters, 32(3), doi:https://doi.org/10.1029/2004GL021586.

Rintoul, S. R. (2018), The global influence of localized dynamics in the Southern Ocean, *Nature*, *558*(7709), 209-218, doi:10.1038/s41586-018-0182-3.

Rodríguez, J. P., et al. (2017), Big data analyses reveal patterns and drivers of the movements of southern elephant seals, Scientific Reports, 7(1), 112, doi:10.1038/s41598-017-00165-0.

Sabu, P., M. P. Subeesh, K. K. Sivakrishnan, and N. Anilkumar (2021), Causes and impacts of anomalous warming in the Prydz Bay, East Antarctica during austral summer 2016-17, *Polar Science*, *30*, doi:10.1016/j.polar.2021.100660.

Schmidtko, S., K. J. Heywood, A. F. Thompson, and S. Aoki (2014), Multidecadal warming of Antarctic waters, Science, 346(6214), 1227-1231, doi:10.1126/science.1256117.

Silvano, A., et al. (2025), Rising surface salinity and declining sea ice: A new Southern Ocean state revealed by satellites, *Proceedings of the National Academy of Sciences*, *122*(27), e2500440122, doi:doi:10.1073/pnas.2500440122.

Silvano, A., et al. (2023), Observing Antarctic Bottom Water in the Southern Ocean, *Frontiers in Marine Science*, *10*, doi:10.3389/fmars.2023.1221701.

Smith, N. R., D. Zhaoqian, K. R. Kerry, and S. Wright (1984), Water masses and circulation in the region of Prydz Bay, Antarctica, *Deep Sea Research Part A. Oceanographic Research Papers*, *31*(9), 1121-1147, doi:10.1016/0198-0149(84)90016-5.

Spence, P., S. M. Griffies, and M. H. England (2014), Rapid subsurface warming and circulation changes of Antarctic coastal waters by poleward shifting winds, *Geophysical Research Letters*, doi:10.1002/2014GL060613.

Stewart, A. L., and A. F. Thompson (2015), Eddy-mediated transport of warm Circumpolar Deep Water across the Antarctic Shelf Break, *Geophysical Research Letters*, *42*(2), 432-440, doi:10.1002/2014gl062281.

Stuecker, M. F., C. M. Bitz, and K. C. Armour (2017), Conditions leading to the unprecedented low Antarctic sea ice extent during the 2016 austral spring season, *Geophysical Research Letters*, *44*(17), 9008-9019, doi:10.1002/2017gl074691.

Swingedouw, D., T. Fichefet, H. Goosse, and M. F. Loutre (2009), Impact of transient freshwater releases in the Southern Ocean on the AMOC and climate, Climate Dynamics, 33(2), 365-381, doi:10.1007/s00382-008-0496-1.

Timmermann, R., S. Danilov, J. Schröter, C. Böning, D. Sidorenko, and K. Rollenhagen (2009), Ocean circulation and sea ice distribution in a finite element global sea ice–ocean model, Ocean Modelling, 27(3), 114-129, doi:https://doi.org/10.1016/j.ocemod.2008.10.009.

Thompson, A. F., K. J. Heywood, S. Schmidtko, and A. L. Stewart (2014), Eddy transport as a key component of the Antarctic overturning circulation, *Nature Geoscience*, *7*(12), 879-884, doi:10.1038/ngeo2289.

Thompson, A. F., A. L. Stewart, P. Spence, and K. J. Heywood (2018), The Antarctic Slope Current in a changing climate, *Reviews of Geophysics*, *56*(4), 741-770, doi:10.1029/2018RG000624.

Timmermann, R., S. Danilov, J. Schröter, C. Böning, D. Sidorenko, and K. Rollenhagen (2009), Ocean circulation and sea ice distribution in a finite element global sea ice–ocean model, *Ocean Modelling*, *27*(3), 114-129, doi:https://doi.org/10.1016/j.ocemod.2008.10.009.

Wang, G., H. H. Hendon, J. M. Arblaster, E.-P. Lim, S. Abhik, and P. van Rensch (2019), Compounding tropical and stratospheric forcing of the record low Antarctic sea-ice in 2016, *Nature Communications*, *10*, doi:10.1038/s41467-018-07689-7.

Wang, Y., M. Zhou, Z. Zhang, and M. S. Dinniman (2023), Seasonal variations in Circumpolar Deep Water intrusions into the Ross Sea continental shelf, *Frontiers in Marine Science*, *10*, doi:10.3389/fmars.2023.1020791.

Whitworth III, T., A. H. Orsi, S.-J. Kim, W. D. Nowlin Jr., and R. A. Locarnini (1985), Water masses and mixing near the Antarctic Slope Front, in *Ocean, Ice, and Atmosphere: Interactions at the Antarctic Continental Margin*, edited, pp. 1-27, doi:https://doi.org/10.1029/AR075p0001.

Williams, G. D., et al. (2016), The suppression of Antarctic bottom water formation by melting ice shelves in Prydz Bay, *Nat Commun*, *7*, 12577, doi:10.1038/ncomms12577.

Wu, Y., Z. Wang, and C. Liu (2021), Impacts of Changed Ice-Ocean stress on the North Atlantic Ocean: role of ocean surface currents, *Frontiers in Marine Science*, *Volume 8 - 2021*, doi:10.3389/fmars.2021.628892.

Yan, D., Z. Lin, Y. Wu, Y. Dai, X. Miao, F. Wu, J. He, and W. Deng (2025), Predicted habitat and area of ecological significance changes for top predators in the Prydz Bay, East Antarctica, under future climate changes, Global Ecology and Conservation, 62, e03697, doi:https://doi.org/10.1016/j.gecco.2025.e03697.

Zhai, X., and D. P. Marshall (2013), Vertical eddy energy fluxes in the North Atlantic subtropical and subpolar gyres, *Journal of Physical Oceanography*, *43*(1), 95-103, doi:10.1175/jpo-d-12-021.1.

Zu, Y. C., L. B. Gao, G. J. Guo, and Y. Fang (2022), Changes of Circumpolar Deep Water between 2006 and 2020 in the south-west Indian Ocean, East Antarctica, *Deep-Sea Research Part Ii-Topical Studies in Oceanography*, *197*, doi:10.1016/j.dsr2.2022.105043.